PHYSICAL REVIEW B VOLUME 7, NUMBER 6 15 MARCH 1973

Molecular-Orbital Treatment for Deep Levels in Semiconductors: Substitutional Nitrogen and the Lattice Vacancy in Diamond

R. P. Messmer and G. D. Watkins
General Electric Corporate Research and Development, Schenectady, New York 12301
(Received 25 May 1972)

A deep-defect level in a semiconductor is simulated by a cluster of host atoms surrounding the defect. The system is then treated as a "large molecule," the energy levels and wave functions for the entire cluster being obtained using molecular-orbital techniques. As examples, the substitutional nitrogen-atom impurity and the lattice vacancy in diamond are treated in some detail. The molecular-orbital technique used in these examples is extended Huckel theory (EHT) and clusters of up to 70 atoms are considered. The results of an EHT treatment of bulk diamond are shown to provide an adequate description of the bands. Lattice relaxations are investigated and shown to be an important part of the deep-level problem. Wave functions are obtained and compared to EPR results for nitrogen in diamond. The agreement between theory and experiment is found to be very good. For the vacancy, the theoretical results are compared to experimental work on the vacancy in silicon. A comparison to the Coulson–Kearsley–Yamaguchi "defect-molecule" treatment of the vacancy is also provided. It is concluded that this cluster approach is a highly promising one for the deep-level problem. Throughout, the physical insight provided by the calculations in understanding the features of the defect centers is stressed.

I. INTRODUCTION

The problem of describing the electronic states of defects and impurities in semiconducting covalent solids is one of great importance, both from a fundamental and practical point of view. The effective-mass theory and corrections to it[1–3] have been highly successful for shallow impurity levels in silicon and germanium. However, for deep levels ($\gtrsim 0.1$ eV from the band edges), which make up a large number of impurity states in covalent solids and practically all defect states produced by radiation damage[4] in these materials, no *general* theoretical description of even moderate success has yet been devised. One complicating feature of the deep-level problem, which is absent in shallow states, is the importance of lattice relaxations and distortions around the defect or impurity in determining the nature of its associated levels.[5,6]

The method of Koster and Slater[7] for treating localized defects has provided valuable insight in application to model problems. However, the generalization of the method[8] needed to treat real defect problems results in rather involved computations since the method is formulated in the Wannier representation. Callaway and Hughes have shown that such calculations are indeed feasible and have investigated the levels produced by the vacancy[8] and divacancy[9] in silicon. Due to the complexity of the calculations, however, the problem was truncated to a small number of perturbed atomic sites, and lattice distortions and relaxations were neglected. More recently, Callaway has estimated the formation energy of the vacancy in silicon,[10] using the same basic approach in conjunction with scattering theory.[11] Parada[12] has also investigated the Pb and Te vacancies in PbTe. Both calculations neglect lattice distortions.

A Green's-function approach closely related to that of Koster and Slater has been proposed by Bassani *et al.*,[13] which provides information about resonant states in addition to the bound states appearing in the gap. Solutions to one-dimensional models were considered. A simple approximate Green's-function approach has been applied to the single vacancy in diamond[14] and silicon.[15] The results, however, seem to be quite sensitive to the various approximations considered.[15] Another method, somewhat related to the Green's-function approach, is the t-matrix formulation of Bennemann.[16] Although his formulation seems to be the most general, in practical application to vacancy and interstitial problems,[16] rather severe approximations are made and lattice distortions neglected.

A rather different approach based on a scattered-wave formalism has been proposed by Beeby[17] and also Johnson.[18] It has the advantage that the explicit knowledge of Wannier or Bloch functions for the perfect crystal is not required. The calculations would be carried out on a cluster of atoms,[19] which would then be "renormalized" by energy-band effects. The method seems to have many advantages, but as yet no calculations have been carried out. Another method using a modified Korringa–Kohn–Rostoker (KKR) theory has been proposed by Grossens and Phariseau,[20] no calculations have been made, however.

All of the approaches mentioned above, with the exception of that of Beeby[17] and Johnson,[18] can be considered from a common viewpoint. That is,

they start with the solutions to the perfect crystal (Bloch functions) and introduce a perturbation (a defect or impurity potential). By using perturbation theory of various forms, they then try to describe the perturbed states using the Bloch functions as a basis set. However, there is a rather different point of view which has been adopted by a number of other authors. In this approach, one starts with the *local environment* of the defect in order to describe the electronic structure of the defect rather than starting with the perfect-crystal states.

The first calculation which used this approach for a defect in a semiconductor was that of Coulson and Kearsley,[21] who treated the vacancy in diamond as a "defect molecule" made up of electrons in the sp^3 "dangling orbitals" from each of the four neighboring atoms. They then constructed many electron states from these orbitals, carried out a configuration interaction calculation, and predicted some optical transitions. Yamaguchi carried out similar calculations for the vacancy[22] and extended them to treat the carbon interstitial in diamond.[23] More recently, similar calculations have been carried out by Coulson and Larkins on the divacancy in diamond[24] and on the vacancy in diamond[25] in somewhat more detail. This approach has also been extended to treat the lattice vacancy in silicon.[26]

In order to evaluate the effect of lattice distortions on the energy states of the Coulson–Kearsley model, the approximation of attaching the "defect molecule" to the rest of the lattice by equilibrium force constants has been used. Although the validity of this procedure is somewhat doubtful, it has enabled the workers who employed it[25–31] to estimate the importance of Jahn–Teller and other relaxation effects.

Another approach which deals only with the local environment of the defect is the point-ion model[32] which has been applied to the diamond vacancy.[26,32,33] However, this model is of questionable validity for covalent solids.

The two general approaches to the problem have therefore been either to start with the infinite crystal states or to start with highly localized defect dangling orbitals. Each approach has provided valuable physical insight into various aspects of the problem. However, neither so far has demonstrated that it can provide a satisfactory theoretical treatment of the deep-level problem. To be specific, a satisfactory treatment must have the following ingredients: (a) it must locate the electronic levels, introduced by the defect or impurity, with respect to the band edges; (b) it must provide wave functions for the electrons in the deep levels which can be compared to experimental information, e.g., EPR studies; (c) it must provide for the possibility of investigating lattice distortions, and relaxation around the defect; and (d) it must be the basis of a practical computational scheme.

The highly localized models emphasize (b) and (c), but supply no information about (a). Also, of course, in constructing a highly localized molecule one is imposing a solution on the problem which may or may not be realistic. Approaches starting from the perfect band states, on the other hand, emphasize (a) but, so far, have supplied little information about (b) or (c). All approaches suffer in various degrees in requirement (d).

We have recently suggested a different approach[34] which is somewhat intermediate between these two extremes and as such embodies many of the advantages of both. The basis of the method is to simulate the problem by a large cluster of host atoms containing the defect. The system is then treated as a "large molecule," the energy levels and wave functions for the cluster being obtained using molecular-orbital techniques. If the cluster can be made large enough to approximate a small crystal, the position of the defect levels can be estimated with respect to the band edges. At the same time, wave functions are produced which have a clear physical interpretation in terms of the local and extended character of the defect. Further, elastic restoring forces are automatically included allowing local lattice relaxations to be handled as an integral part of the treatment. Finally, useful semiempirical molecular-orbital schemes exist which allow sizable clusters to be handled with modest computing times. Such an approach therefore appears highly promising, satisfying to some extent each of the above requirements.

The concept of a cluster approach is not new. Very early Inui and Uemura[35] described what they termed the "large-molecule" approach to the F center in the alkali halides. Here they expanded a linear-combination-of-atomic-orbitals (LCAO) model involving the near neighbors of the negative-ion vacancy to include the effective crystalline field produced by the next neighbors. More recently, Birman[36] and Walter and Birman[37] treated the copper impurity in ZnS by using a cluster consisting of the central copper atom surrounded by four $S(Zn)_3$ groups to represent the host lattice. They employed the molecular-orbital treatment of Wolfsberg and Helmholtz[38] in an attempt to match the copper d-level splittings and their electrical level position in the ZnS band gap.

A cluster approach has also been used to calculate the *physical* properties of defects in solids. In particular, Moore and Carlson[39] used extended Huckel theory[40,41] on a 24-atom cluster of carbon atoms arranged in the graphite lattice to obtain activation energies for vacancy migration and

Frenkel-pair formation. They did not investigate the electronic properties of the defects, however.

Our approach therefore represents a logical extension of the work of Birman and Moore and Carlson. We will take larger clusters than Birman to better match the more extended electronic states of the solid. However, the basic concept is the same. At the same time we will take advantage of the fact that elastic properties of the cluster are also described, as in the work of Moore and Carlson, to treat lattice relaxations around the defect.

It is this molecular-cluster approach to the deep-level problem which we wish to discuss in this paper. As examples, we will explore in detail its application to two model problems: (i) the substitutional nitrogen donor and (ii) the lattice vacancy in diamond. The outline of the presentation is as follows. In Sec. II we detail the molecular-cluster description and choose a particular molecular-orbital (MO) approximation, extended Huckel theory (EHT). In Sec. III we consider the elastic and electronic properties calculated for a diamond cluster in the absence of a defect. Also in Sec. III we explore the problems associated with the finite size of the cluster, its surfaces, etc., by comparing the electronic states of the cluster to those of the infinite crystal, as determined from a band-structure calculation using the same MO method. Comparison of these results in turn to *ab initio* band-structure calculations are used as a test of the validity of the MO method. Problems associated with charge distribution and self-consistency in the MO treatment are also considered. In Sec. IV results of calculations on the nitrogen donor are presented and compared to experiment. In Sec. V results on the lattice vacancy are described and in Sec. VI a summary of the main conclusions are given.

II. DESCRIPTION OF MOLECULAR CLUSTER

First let us consider a perfect *infinite* crystal whose electronic structure we choose to represent by using an LCAO approach. The one-electron crystal orbitals ϕ_i will be given as

$$\phi_i = \sum_\nu c_{\nu i}\,\chi_\nu\,, \tag{1}$$

where the χ_ν are the atomic orbitals and the index ν runs over all atomic orbitals on each atom and over all atoms. The $c_{\nu i}$ are the solutions to the one-electron Hartree–Fock equations for the crystal, which are

$$\sum_\nu^{\infty}(F_{\mu\nu} - S_{\mu\nu}\epsilon_i)c_{\nu i} = 0\,, \quad i = 1, 2, \ldots, \infty\,. \tag{2}$$

The ϵ_i are the one-electron crystal-orbital energies; $F_{\mu\nu}$ is the matrix element between atomic orbitals μ and ν with respect to an effective one-electron operator F, and $S_{\mu\nu}$ is the overlap integral between these atomic orbitals.[42] This infinite set of equations can be reduced, or to put it another way, the square matrices $F_{\mu\nu}$ and $S_{\mu\nu}$ of infinite dimensions can be factorized by taking account of translational symmetry. The resultant set of reduced equations can be solved to give an accurate band structure of the perfect solid.[43] However, if the solid is not perfect, i.e., if there is a defect or impurity in the lattice, then the translational symmetry of the perfect crystal no longer exists and the set of Eqs. (2) can no longer be simplified on this basis.

Therefore, in order to treat an impurity or defect in the solid, we must start with the whole set of Eqs. (2). But then let us focus our attention on the defect or impurity and its local environment. If we start with the defect and include a large number of atoms surrounding it, we should obtain a good description of the defect problem. In the limit of including *all* the bulk atoms surrounding the defect, we would, of course, be solving Eq. (2) exactly. However, from a practical point of view, the latter problem is impossible to solve. We therefore restrict ourselves to the consideration of a finite number of host atoms surrounding the defect. In this case, Eqs. (2) reduce to a finite number:

$$\sum_\nu^{N}(F_{\mu\nu} - S_{\mu\nu}\epsilon_i)c_{\nu i} = 0\,, \quad i = 1, 2, \ldots, N\,. \tag{3}$$

The value of N will depend upon the number of host atoms included in the cluster. The solutions of Eq. (3) give the molecular orbitals and their energies for the molecular cluster. The larger the molecular cluster, the better the approximation Eqs. (3) will be to the Eqs. (2).

This method we have just outlined satisfies conditions (a)–(c) described in Sec. I. However, for a cluster larger than about 15 atoms, condition (d) is not satisfied. That is, the computational part of the scheme becomes too burdensome. In order to circumvent this difficulty, we must make approximations in Eqs. (3). This is the essence of the method we have proposed[34]: *Apply Eqs.* (3) *to a molecular cluster representing a defect and its surroundings and use an appropriate molecular-orbital technique to simplify Eqs.* (3). In the preliminary applications of this method,[33,44–46] we have chosen a particularly simple approximate MO scheme, namely, the extended Huckel theory.[40,41] We will now discuss briefly this MO scheme and in Sec. III show that even with the approximations it imposes on Eqs. (3), the resultant equations satisfy conditions (a)–(d).

A. Extended Huckel Theory

Extended Huckel theory[40,41] is a noniterative approximation to Eqs. (3).[47] We can completely

specify the method by giving the explicit form of the matrix elements $F_{\mu\nu}$:

$$F_{\mu\nu} = -\tfrac{1}{2} K_{\mu\nu}(I_\mu + I_\nu) S_{\mu\nu} , \tag{4}$$

where μ and ν are valence orbitals only and where

$$K_{\mu\nu} = \begin{cases} K & \text{for } \mu \neq \nu \\ 1 & \text{for } \mu = \nu . \end{cases} \tag{5}$$

Here $1 < K < 2$ and is an adjustable parameter (usually $K = 1.75$ in applications to organic molecules[40]), I_μ is the μth valence-orbital ionization potential,[48,49] and $S_{\mu\nu}$ is the overlap integral between two Slater-type atomic orbitals. The radial part of the Slater-type orbital is given by

$$\chi_\mu = N_\mu r^{n-1} e^{-\zeta r} , \tag{6}$$

where N_μ is a normalization constant, n is the principal quantum number of the orbital μ, and ζ is an orbital exponent obtained for the calculations to be presented here by Slater's rules.[50] A measure of the total energy of the system is given by the sum of the energies of all the occupied one-electron molecular orbitals. That is,

$$E_{\text{tot}} \cong \sum_i n_i \epsilon_i , \tag{7}$$

where ϵ_i is the energy and n_i the occupation number of the ith orbital.

The total energy of the system of course is *not* rigorously given by Eq. (7). It should be corrected by the subtraction of two-electron terms and the addition of nuclear-nuclear core-repulsion terms. However, in the EHT method, explicit account is not taken of either the electron-electron repulsion or nuclear-nuclear repulsion terms; therefore, the correction terms to Eq. (7) are not well defined. Fortunately, studies on the deformation of molecules[40,51,52] have shown that arguments based on Eq. (7) often turn out to be quite good. The reason for this has been discussed by a number of workers.[53,54] It results from a tendency for these two terms to cancel each other, particularly as regards their variation with the internuclear framework as reflected in the elastic properties of the molecule. This cancellation is best for molecules of low ionicity. For instance, the studies of Allen and Russell[51] and Allen[52] show that in *ab initio* calculations the actual total energy and $\sum_i n_i \epsilon_i$ considered as a function of bond angles have parallel behavior for molecules whose constituents are relatively close in electronegativity. Allen also shows that Eq. (7), used with EHT, is a good approximation to this behavior and thus, for systems with a relatively uniform distribution of charge between the atoms, predicts reasonably good values for the equilibrium bond angles. Also, more specifically, we will show in Sec. III that for a cluster of carbon atoms on the diamond lattice, the elastic properties inferred by Eq. (7) are remarkably close to the experimental diamond values. This gives us confidence that Eq. (7) can be used in treating lattice distortions. The fact that successful predictions using EHT depend upon a relatively uniform charge distribution has also been pointed out by Blyholder and Coulson.[55]

A few words should also be mentioned with regard to the effects of the trunctation of the infinite matrix to a finite size. Since EHT is a noniterative scheme, the matrix elements $F_{\mu\nu}$ will not be modified due to surface effects as they would be in a self-consistent procedure. A fully self-consistent procedure would give a solution to the *cluster per se*, which we are not interested in. Therefore, a scheme like EHT has the advantage that it is more appropriate to the bulk than the cluster *per se*, and that in this way the calculation is in some ways a better approach to the problem than a fully self-consistent treatment of the cluster. These points will become clearer in the discussions of calculations in Sec. III.

III. EHT CALCULATIONS IN ABSENCE OF DEFECT

For most of the calculations to be described, we have used the 35-atom cluster of carbon atoms shown in Fig. 1. The cluster includes a central atom plus all of its first (1, 1, 1), second (2, 2, 0), third (3, 1, $\bar{1}$), and fourth (4, 0, 0) nearest neighbors in the diamond lattice. The choice of this cluster represents a compromise between the obvious desire, on the one hand, to have it as large as possible and the practical limitations, on the other hand, of the computing time and core storage required in the calculations.[56]

In the calculations, the atomic orbitals were taken to be one $2s$ and three $2p$ Slater orbitals on each carbon atom. The exponent ζ [Eq. (6)] for both orbitals was taken to be[50] 1.625. The valence-orbital ionization potentials I_μ were 19.44 and 10.67 eV for the $2s$ and $2p$ orbitals, respectively.[48,49] The constant K in Eq. (5) was taken to be[40] 1.75. The input parameters were therefore determined in advance entirely from atomic data (I_μ and ζ) or small-molecule calculations (K) and were not empirically adjusted in any way to reflect the diamond properties.

A. Effect of Cluster Size, Surfaces, etc.

In Fig. 2 we show the calculated molecular-orbital energies as a function of the size of the cluster, starting from a central carbon atom and then adding successive shells. Also shown is the result for the infinite cluster, determined by an EHT band-structure calculation[57] using the identical parameters. We see immediately that as the size of the cluster increases, the "band structure" begins to emerge, with the bonding MO's grouped

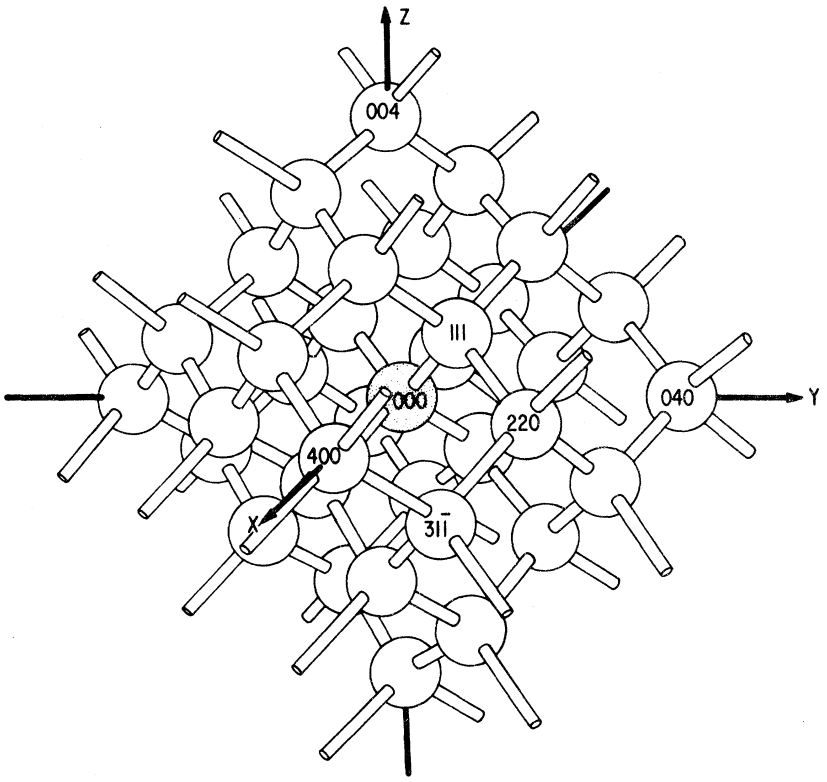

FIG. 1. 35-atom cluster used for most of the LCAO-MO calculations.

into what can be identified as a valence band, the antibonding MO's forming a conduction band, and with a forbidden gap between.

The bonding molecular orbitals appear to converge to the infinite valence-band width rather quickly, the 35-carbon-atom width (measured as the difference between the highest and lowest energy states) already giving 20.7 eV compared to 21.5 eV for the infinite cluster. The bottom of the conduction band on the other hand, and correspondingly the band gap, converge to their infinite values somewhat more slowly. For the 35-atom cluster, the band gap is 9.5 eV compared to the infinite value of 4.7 eV. For the 71-atom cluster, the band gap is 7.4 eV.

A closer look at the valence-band states reveals one reason for its more rapid convergence. For each cluster there are S more orbitals in what we have called the valence band than in the conduction band, where S is the number of dangling bonds on the surface. The "surface states" associated with these dangling bonds have therefore turned out in this model to be energetically within the valence band. This is not surprising. An isolated carbon $2p$ orbital has an energy $-I_\mu = -10.67$ eV, which is well below the infinite-cluster band edge of -8.73 eV. As a result such an orbital on the surface should admix with the bulk valence-band states and tend to become delocalized, penetrating into the bulk. In effect, the effective "size" of the cluster for the valence band is larger, extending beyond the surface atoms into the space occupied by these surface orbitals. For the conduction band, however, this space is not available, the wave functions being restricted to the region between the atoms, and the effective "size" of the cluster is smaller.

Figure 3 shows the electronic states near the top of the valence band on an expanded scale. In all cases for clusters of 17 or more atoms, states exist which are above the top of the infinite cluster valence-band edge. This must be a result of the surfaces. For some clusters, the corresponding wave functions reveal a greater concentration on the surface atoms and thus they can be viewed as "surface states." However, for the 35-atom cluster, the uppermost t_2 state is found to be spread quite uniformly throughout the cluster, suggesting it to be viewed as a bulk state whose energy has been shifted by confining it to the small cluster.[59]

There are several ways that one might attempt to reduce surface effects and better simulate the infinite crystal at the boundaries. Carlson and Moore[60] have suggested tying up the surface orbitals with bonds to hydrogen atoms as they had done previously on graphite calculations.[39] Such a modification has recently been performed for the

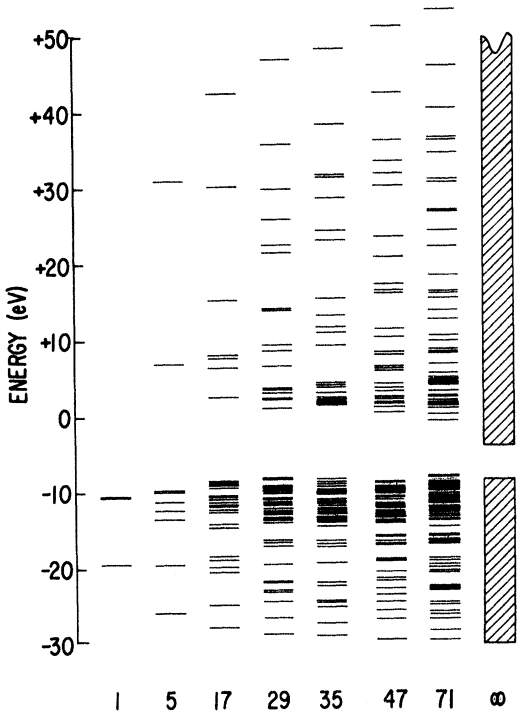

FIG. 2. Energies of the one-electron MO's for a diamond cluster as a function of cluster size, starting with the central atom (1) and adding successive shells of neighbors up to and including the sixth-nearest-neighbor shell (71). The result for the infinite cluster comes from a band-structure calculation using the same EHT parameters.

35-atom cluster by Larkins.[61] He finds, for instance, that the band gap is reduced from 9.5 to 8.5 eV with the hydrogens. Another approach would be to place periodic boundary conditions on a cluster. We are currently using this approach on a 64-atom cluster and these results will be the subject of a future publication.

In the present paper, however, we will use the 35-atom cluster of Fig. 1 and we will not attempt to "tie up" the surface orbitals in any way. We conclude from the preceding discussion that such a cluster actually does a rather good job of simulating the valence-band states of the infinite crystal. There are, however, effects of the surfaces; for example, in some cases "surface states" exist, and "truncation effects" can serve to shift the energies of the bulk states somewhat. However, they are not great, being apparently rather less than ~1 eV, as seen in Fig. 3. The effects on the conduction-band edge, on the other hand, are somewhat greater. We expect, therefore, that our treatment of localized defects may be somewhat more reliable for states near the valence-band edge than for those near the conduction-band edge.

B. Validity of EHT

In Sec. III A, we considered the approximations resulting from truncating the problem to a finite cluster. A second question is how well EHT actually approximates the correct Hartree–Fock solutions, Eqs. (2) and (3); and, in particular, how well such a simple tight-binding LCAO-MO approach can reproduce the more extended states of the bulk crystal. This question can be separated from the approximations involved in truncation to a finite cluster by comparing the band structure calculated using EHT with that obtained by *ab initio* methods. The band-structure solution is, of course, the solution of the infinite cluster, with no surfaces.

The band-structure calculated[57] using EHT, with

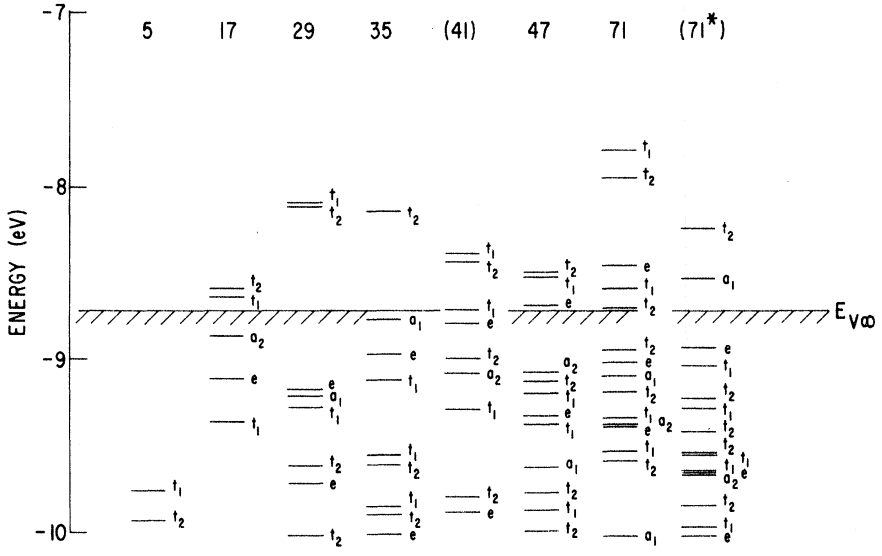

FIG. 3. Expanded view of the states near the top of the valence-band edge for a diamond cluster vs cluster size. In addition to the simple progression of adding successive neighbor shells (Fig. 2) we include a 41-atom cluster which is made up of first, second, third, and fifth shells (Ref. 61), and a 71*-atom cluster constructed to have only (111) surfaces (Ref. 58).

the identical parameters as used in the cluster calculations, is shown in Fig. 4(a). For comparison, a recent *ab initio* calculation by Painter *et al.*[62] is shown in Fig. 4(b). This comparison is given in more detail in Table I for several points in the Brillouin zone. We note that the EHT results agree remarkably well with those of the *ab initio* treatment for all of the valence bands. Some of the conduction bands as defined by L_3, Γ_{15}, and X_3 also agree well.

On the other hand, certain features of the conduction band appear quite poorly described. In particular, the conduction-band width is much too large and the minimum in the conduction band in the $\langle 100 \rangle$ direction is not reproduced. These features reflect a poor description of the bands associated with X_1, $\Gamma_{2'}$ and L_1, $L_{2'}$.

In spite of this poor agreement on two of the four conduction bands, the over-all agreement must be considered surprisingly good when one considers that the EHT parameters have been determined in advance entirely from atomic data (I_μ, ζ) and small-molecule properties (K) and have not been adjusted in any way to match the diamond properties.

In this regard, it is instructive to compare these results to those of a recent pseudopotential calculation,[63] also given in Table I, which employed six parameters empirically adjusted to match selected symmetry points in the diamond band structure. It is apparent that EHT actually does a much better job of matching the valence band and the two conduction bands associated with Γ_{15}, X_3, and L_3 than does the pseudopotential method. The pseudopotential values, on the other hand, are considerably better for $\Gamma_{2'}$, X_1, and $L_{2'}$, but, of course, these particular points are empirically matched.

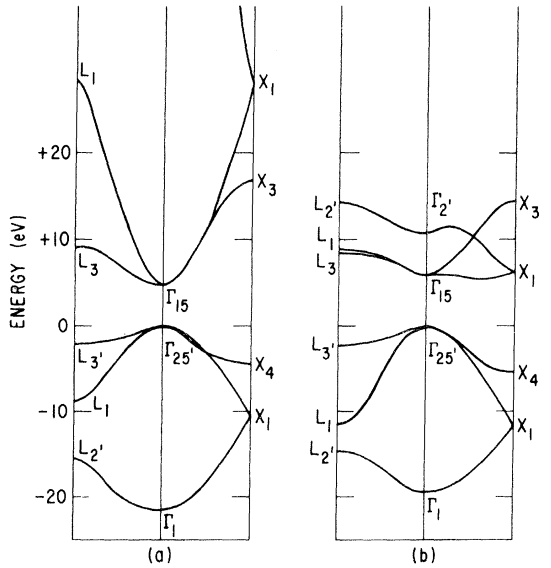

FIG. 4. Comparison of the diamond band structure (a) calculated by EHT, with (b) *ab initio* results of Painter *et al.* (Ref. 62). The zero of energy has been shifted in each case to coincide with the $\Gamma_{25'}$ point.

TABLE I. Comparison of band structure of diamond calculated by EHT with that of other methods (energies in eV). The zero of energy in each case has been shifted to coincide with the $\Gamma_{25'}$ point.

Symmetry point	EHT	*ab initio*[a]	Pseudopotential[b]
Valence bands			
$\Gamma_{25'}$	0.0	0.0	0.0
Γ_1	−21.5	−19.6	−29.1
X_4	−4.4	−5.3	−6.0
X_1	−10.5	−11.6	−19.6
$L_{3'}$	−2.3	−2.4	−2.8
L_1	−9.0	−11.7	−15.9
$L_{2'}$	−15.4	−14.5	−24.3
Conduction bands			
Γ_{15}	+4.7	+6.0	+8.1
X_3	+16.8	+14.3	>26.0
L_3	+9.1	+8.9	+10.3
$\Gamma_{2'}$	+69.8	+10.8	+6.9
X_1	+28.1	+6.3	+5.9
L_1	+28.3	+8.2	>20.0
$L_{2'}$	+46.5	+14.1	+5.6

[a]G. S. Painter, D. E. Ellis, and A. R. Lubinsky, Phys. Rev. B 4, 3610 (1971).

[b]L. A. Hemstreet, C. Y. Fong, and M. L. Cohen, Phys. Rev. B 2, 2054 (1970). The values given here have been estimated from Fig. 1.

We therefore interpret the agreement in Fig. 4 and Table I to indicate that EHT, in the simple form which we use for the defect cluster calculations to follow, reproduces enough of the essential features of the perfect-crystal band states to provide a meaningful "connection" between a localized-defect state (for which the LCAO approach is clearly meaningful) and the perfect-lattice states (i.e., band edges, etc.).

It should be mentioned that the agreement with the band structure can be improved considerably by small adjustments of some of the EHT parameters, as has recently been pointed out by one of us (R. P. M.).[57] In future publications, we will explore such empirically adjusted EHT parameters as possibly providing a better starting point for defect calculations. In this paper, however, we will make no such adjustments of parameters in the calculations.

C. Elastic Properties

As described in Sec. II, a measure of the total energy of the system is given by

$$E_{\text{tot}} \cong \sum_i n_i \epsilon_i \,, \tag{7}$$

where n_i is the occupation number and ϵ_i the energy of the ith MO. In this section we will investigate the elastic properties implied by (7).

In evaluating Eq. (7) for a cluster, our procedure will be to fill all of the "valence-band" orbitals. This means, of course, that we are also filling the S "surface" orbitals. This must be done because, as discussed in Sec. III A, these orbitals are not really distinguishable. All of the "valence-band" orbitals have some surface and some bulk character and it is necessary that all of them be occupied in order to completely fill the bulk states.

We note that in following this procedure, we are not dealing with a "neutral" cluster, but rather have added S additional electrons (36 for the 35-carbon-atom cluster), and the cluster carries a net charge of $-Se$. One might have been tempted instead to make the cluster neutral. If this were done, however, there would be partially filled, closely spaced states near the top of the "valence band" which would reflect the elastic softness of the cluster surfaces. Since we are not interested in the cluster *per se*, but are rather using it only as a means of approximating the larger bulk system, filling all of the valence-band orbitals to a large extent avoids these extraneous surface effects.

We calculate the change in energy (7) per unit volume of the cluster for each of three small-uniform-distortion modes: (i) hydrostatic (A_1), (ii) tetragonal (E), and (iii) trigonal (T_2). For this, we define the effective volume of the cluster to be $(N-\frac{1}{4}S)V_0$, where V_0 is the volume per atom (5.65 Å^3), N is the number of atoms, and S is the number of surface orbitals. These results, in conjunction with conventional elasticity theory,[64] allow evaluation of the elastic constants c_{11}, c_{12}, and c_{44}.

The results for the 35-atom cluster are given in Table II along with experimentally measured values for diamond. The agreement is seen to be remarkably good. The fact that all elastic constants are successfully calculated means that not only are "bond-bending" force constants reproduced, as discussed by Allen *et al.*[51,52] (Sec. II), but bond-stretching force constants as well. For instance, the bulk modulus B obtained from the A_1 hydrostatic compression mode is pure bond stretching. We conclude, therefore, that through Eq. (7), the model contains elastic forces which are realistic.[65–68] We will take advantage of this to treat lattice relaxations around a defect.

TABLE II. Comparison of calculated (EHT) and observed elastic constants (10^{12} dyn/cm^2) for diamond.

	EHT	Experimental
c_{11}	8.6	10.76[a]
c_{12}	2.7	1.25,[a] 2.75[b]
c_{44}	5.0	5.76[a]
$B=\frac{1}{3}(c_{11}+2c_{12})$	4.6	4.4[a]

[a]H. J. McSkimin and W. L. Bond, Phys. Rev. 105, 116 (1957).

[b]Markham, as reported in *Physical Properties of Diamond*, edited by R. Berman (Oxford U.P., London, 1965), p. 415.

The 35-atom cluster is stable against E and T_2 distortions, the total energy rising quadratically with strain for small distortions. This is not true for the hydrostatic A_1 mode, however, which also exhibits a linear change with distortion. In calculating the elastic constants, we have therefore determined $B=\frac{1}{3}(c_{11}+2c_{12})$ from the quadratic part of the dependence, which is, of course, that part of the energy that reflects the elastic properties of the cluster.

The existence of a linear term means that the cluster is actually not "stable" at the experimentally observed interatomic separation (1.54 Å) for which the calculations were performed. Allowing the lattice to relax for minimum energy (7), we find that the lattice expands 19%. At this separation, the agreement of calculated elastic constants and band structure with the diamond properties is poorer. We have elected, therefore, in all of our calculations to fix the atoms initially at their normal experimental positions and treat only distortions that maintain constant volume for the cluster. This is automatically satisfied for all except those of A_1 symmetry. With caution, we will also treat local A_1 modes around a defect, but in doing so, we will constrain the outer shells from expanding or contracting. (We are, in effect, cancelling the linear term in the energy by applying the necessary external "force" to hold the outer shells of atoms in their proper positions.)

This failure of EHT to predict correct equilibrium bond distances was first pointed out by Hoffmann.[40] He found that the predicted single bond C-C equilibrium distance was too large (~25% in ethane). This is in large part the reason that the bond angle predicting properties of EHT have been emphasized. Our results demonstrate, however, that the bond-stretching force constants, as well, can be accurately reproduced by EHT (at least in certain cases) when the atoms are held at their proper internuclear separation.

D. Further Discussion

As discussed in Sec. II A, the success of EHT depends upon a relatively uniform charge distribution existing over the atoms (low ionicity). This is basically because EHT is not a self-consistent treatment. It works well for pure covalent bonds between atoms, but cannot properly handle ionic

bonds where a significant amount of charge is transferred from one atom to another. So far, we have used it here, therefore, under the ideal circumstances; i.e., a cluster of identical atoms, for which the correct solution, at least for the infinite cluster, must be a completely uniform charge distribution.

In the defect studies to follow, however, we will consider replacing one of the carbon atoms with an impurity atom. As the electronegativity difference increases between the impurity atom and its carbon neighbors, we anticipate that EHT will become an increasingly poorer approximation—at least for the immediate environment of the impurity. As a guide, we note that Allen has concluded that when the electronegativity difference between a pair of adjacent atoms exceeds about 1.3 on the Pauling scale[69] or 1.0 on the Sanderson scale,[70] EHT begins to fail as regards its ability to predict "bond-bending" elastic properties.[51] The impurity that we will treat is nitrogen, which has a difference from carbon of ~0.5 on either scale. We tentatively conclude, therefore, that, if used and interpreted cautiously, EHT can continue to provide a useful approximation for impurities such as nitrogen as well. A Mulliken charge-population analysis[71] of the cluster is performed for each calculation and serves as a useful monitor of charge distribution. In the defect calculations to follow, this can be used as an indicator of the degree to which problems may exist from this source.

As described in Sec. III C, our procedure of filling all of the valence-band orbitals is equivalent to adding 36(S) extra electrons to the cluster. A Mulliken population analysis reveals that this extra charge resides primarily on the surface atoms with the (2, 2, 0) and (3, 1, $\bar{1}$) atoms having a net charge of $\sim -e$ and the (4, 0, 0) atoms, $\sim -2e$. We have in effect put an extra electron on each surface dangling bond to saturate it. Therefore, in the analysis to follow, we will define as "uniform charge density" that distribution which gives an extra electronic charge on a surface atom for each of its dangling bonds. Departures from this will be taken as evidence of ionicity.

It is important to remember that this procedure of filling the orbitals is purely a computational one after the calculation. It in no way affects the wave functions or electric level positions of the orbitals. The apparent concentration of charge that results from this procedure in no way affects the validity of the EHT approximation because in the real crystal, with no surfaces, and no excess charge, the charge distribution will be uniform.

Finally, since EHT is not a self-consistent treatment it approximates best the neutral charge state of the defect, where the charge density is relatively uniformly distributed over the system.

IV. SUBSTITUTIONAL NITROGEN IN DIAMOND

Substitutional nitrogen is the only point defect in diamond for which detailed unambiguous experimental information is available and as such it serves as a key test for our theoretical approach. Nitrogen is known to introduce a deep donor level which, from photoconductivity,[72] and luminescence studies[73] is estimated to be at $\sim E_c - 4.0$ eV, or only about 1.5 eV above the valence-band edge.[74]

The reason for its being so deep has been a mystery of considerable concern in the literature. Nitrogen in diamond is the direct counterpart of phosphorus in silicon, which is a shallow donor at $\sim E_c - 0.05$ eV. A simple extension of the Kohn–Luttinger effective-mass treatment,[2,3] which has been so successful for shallow donors in silicon, predicts, for the nitrogen in diamond,[28] $E_c - 0.4$ eV. This is a full order of magnitude lower than the experimental estimate. The effective-mass treatment therefore appears to fail completely in this case.

A great deal is known as well about the microscopic structure of the defect from EPR[75–78] and electron-nuclear-double-resonance (ENDOR)[79] studies. In particular, a large trigonal Jahn–Teller distortion has been inferred for the defect. In addition, analysis of the EPR and ENDOR results has given detailed information about the wave function of the donor state.

In Fig. 5(b), we show the one-electron molecular-orbital energies that result from the calculation when the central atom of the 35-atom cluster is replaced by nitrogen (Slater exponent 1.95, ionization potentials 25.58 and 13.19 eV for the 2s and 2p orbitals, respectively[49]). A triply degenerate orbital now appears in the forbidden gap, having emerged from the conduction band. It is approximately 1.5 eV below the conduction-band edge of the cluster and the molecular-wave-function coefficients $c_{\nu i}$ reveal that it is highly localized on the nitrogen and its immediate carbon neighbors. Because neutral nitrogen has five valence electrons (one more than carbon), this orbital will be singly occupied in the "neutral" cluster. We therefore identify it as the nitrogen donor state.

Because the donor state is triply degenerate, it is a candidate for a Jahn–Teller distortion. Let us therefore investigate this at the outset.

A. Jahn–Teller Distortion

As is usual in the treatment of Jahn–Teller problems, a substantial simplification is acheived by taking advantage of the symmetry of the problem. In our case, the point group symmetry of the cluster is T_d, and each of the molecular-orbital wave functions can be classified according to the irreducible representations A_1, A_2, E, T_1, or T_2

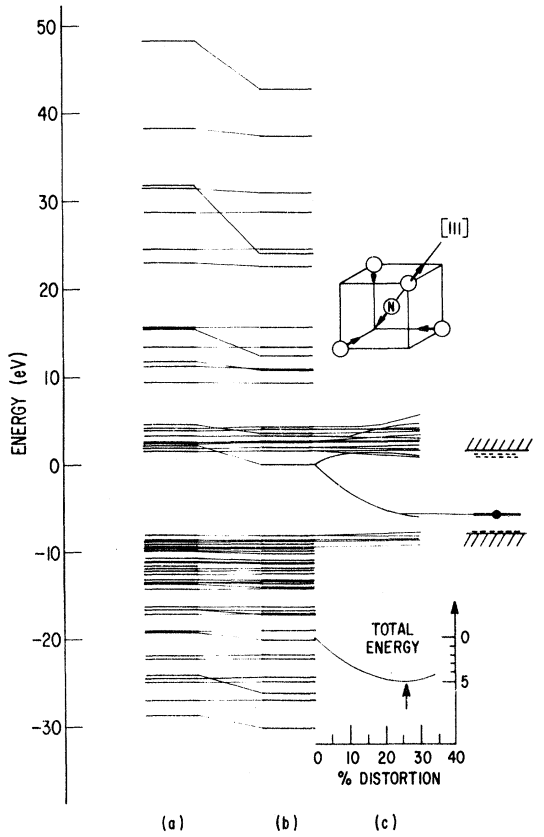

FIG. 5. (a) Energies of the one-electron MO's for a 35-carbon atom "diamond." (b) Energies with nitrogen as the central atom, no lattice relaxation. (c) Effect of trigonal Jahn–Teller distortion. The total energy has a minimum when the amplitude of the normalized distortion mode (shown in inset) is 26.2% of the nearest-neighbor distance. The distortion causes a lowering of the donor level to $E_v + 2.2$ eV.

of the T_d group. The completely filled valence band must transform according to A_1 so that the transformation properties of the wave function of the total system are simply those of the singly occupied one-electron MO donor state in the gap. By inspection of the molecular-wave-function coefficients c_{vi} for this orbital, it is found to be T_2.

The distortions of the cluster can also be classified according to their symmetry. For an electronic state belonging to the irreducible representation Γ, only those distortions whose symmetry is contained in the symmetric direct product $[\Gamma \times \Gamma]$ can give rise to a linear shift or splitting of the energy states vs distortion, a necessary requirement for lattice relaxation involving these modes to occur.[80] For an electronic state T_2, $[T_2 \times T_2] \supset A_1 + E + T_2$. The A_1 modes are symmetric "breathing" modes that do not lower the symmetry and are therefore not associated with the Jahn–Teller effect. (We will return to these modes later.) The Jahn–Teller modes are therefore of E and T_2 symmetry.

There are many E and T_2 modes associated with the cluster and the problem is still potentially a very complex one. However, because the defect wave function is highly localized, the distortions should also be primarily local ones. We will therefore limit ourselves in this treatment to the distortions associated with the nitrogen atom and its four nearest carbon neighbors only.

A set of normalized symmetry modes of distortion for these five atoms are given in Fig. 6. The A_1, E, and T_2 modes correspond to the normal modes for four isolated carbon atoms located at the nearest-neighbor positions. The T_2' mode describes in turn the vibrational motion of the central nitrogen atom alone. There are therefore only two modes of T_2 symmetry and one mode of E symmetry which must be considered.

The problem of a T_2 electronic state coupled to E and T_2 modes of distortion has been treated in considerable detail in the literature[80–82] and will not be repeated here. In our case, the complete solution would lead to three complex energy surfaces in the eight-dimensional space spanned by the two E distortion coordinates and six $T_2 + T_2'$ coordinates. However, since we are interested here only in the minimum-energy configuration, the

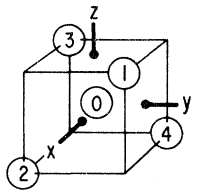

$$A_1 \quad Q_1 = \frac{1}{\sqrt{12}}(u_1+u_2-u_3-u_4+v_1-v_2-v_3+v_4+w_1-w_2+w_3-w_4)$$

$$E \begin{cases} Q_\theta = \frac{1}{\sqrt{24}}(-u_1-u_2+u_3+u_4-v_1+v_2+v_3-v_4+2w_1-2w_2+2w_3-2w_4) \\ Q_\epsilon = \frac{1}{\sqrt{8}}(u_1+u_2-u_3-u_4-v_1+v_2+v_3-v_4) \end{cases}$$

$$T_2 \begin{cases} Q_x = \frac{1}{\sqrt{8}}(v_1-v_2+v_3-v_4+w_1-w_2-w_3+w_4) \\ Q_y = \frac{1}{\sqrt{8}}(u_1-u_2+u_3-u_4+w_1+w_2-w_3-w_4) \\ Q_z = \frac{1}{\sqrt{8}}(u_1-u_2-u_3+u_4+v_1+v_2-v_3-v_4) \end{cases}$$

$$T_2' \begin{cases} Q_x' = u_0 \\ Q_y' = v_0 \\ Q_z' = w_0 \end{cases}$$

FIG. 6. Set of normalized symmetry modes of distortion for the central nitrogen (0) and four nearest-neighbor carbon atoms (1, 2, 3, 4) used in the Jahn–Teller calculation. The displacement coordinates of atom i are (u_i, v_i, w_i).

problem is greatly simplified. In particular, it has been demonstrated that the lowest-energy state is a singlet electronic state produced by either a pure-tetragonal (E mode only) or pure-trigonal (T_2 modes only) distortion depending upon whether the coupling to the E or T_2 modes dominate, respectively.[81] We can therefore investigate each of these modes separately.

For the tetragonal mode, we take Q_θ (see Fig. 6). For the trigonal modes we take the linear combinations

$$Q_a = 3^{-1/2}(Q_x + Q_y + Q_z)\,,$$
$$Q_a' = 3^{-1/2}(Q_x' + Q_y' + Q_z')\,, \tag{8}$$

associated with distortions along the [111] direction. For small amplitudes of each of these modes ($Q_{\Gamma i}$), the T_2 electronic state splits linearly with distortion into a singlet ($-V_\Gamma Q_{\Gamma i}$) and a doublet ($+\frac{1}{2}V_\Gamma Q_{\Gamma i}$), where V_Γ is the Jahn–Teller coupling coefficient for the mode of Γ symmetry. The energy for the singlet state can then be written

$$E = -V_\Gamma Q_{\Gamma i} + \tfrac{1}{2}k_\Gamma (Q_{\Gamma i})^2 + \cdots\,. \tag{9}$$

A simple calculation with a small amplitude distortion (~1%) for each mode is therefore sufficient to estimate both V_Γ and k_Γ, V_Γ being given as $\frac{2}{3}$ the energy splitting produced in the t_2 molecular orbital and k_Γ being derived from (9) using the total energy. The results for each mode are given in Table III.

We note that the coupling coefficients V_Γ to the trigonal modes are substantially larger than the tetragonal one indicating that a trigonal distortion should take over. To further simplify the problem, we now construct two new orthogonal sets of trigonal modes as follows:

$$Q_a^\alpha = (V_A Q_a + V_A' Q_a')/(V_A^2 + V_A'^2)^{1/2}\,,$$
$$Q_a^\beta = (V_A' Q_a - V_A Q_a')/(V_A^2 + V_A'^2)^{1/2}\,, \tag{10}$$

where A designates the T_2 representation. In doing this, the linear coupling coefficient to Q_a^β is made zero and we approximate the problem as that of coupling to a single trigonal mode[83] Q_a^α

$$E = -\bar{V}_A Q_a^\alpha + \tfrac{1}{2}\bar{k}_A (Q_a^\alpha)^2 + \cdots\,, \tag{11}$$

where

$$\bar{V}_A = (V_A^2 + V_A'^2)^{1/2}\,. \tag{12}$$

The Q_a^α mode is illustrated in Fig. 5(c).

We now perform the EHT calculation for the cluster as a function of the amplitude of this Q_a^α trigonal mode. The results for the molecular-orbital energies near the gap and the total EHT energy are given in Fig. 5(c). We see that a very large Jahn–Teller distortion is predicted. The total stabilization energy is ~5.0 eV. The amplitude of the distortion that minimizes the total energy is 0.4 Å, or 26.2% of the nearest-neighbor distance (1.54 Å). Further, we note that the nitrogen donor state has dropped to within 2.2 eV of the valence band.

TABLE III. Jahn–Teller coupling coefficients (V_Γ) and local force constants (k_Γ) determined for the 34C+N and 35C clusters.

Mode (Γ)	34C+N V (eV/Å)	34C+N k (eV/Å^2)	35C k (eV/Å^2)
E	+5.1	15.5	(32.4)
T_2	+10.1	−2.1	(26.0)
T_2'	−18.3	1.9	(30.9)

Our results, therefore, provide for the first time a simple explanation of why the nitrogen donor state is so deep. In our model, it is the direct consequence of a large Jahn–Teller distortion. One of us (G. D. W.)[5] has previously pointed out that Jahn–Teller effects can be important in determining the electrical level position of a deep level in the gap. However, we believe the results we present in this paper represent the first quantitative demonstration of this point.

Experimentally, it is known from EPR studies that the nitrogen does indeed undergo a trigonal Jahn–Teller distortion.[75–78] The magnitude of the distortion has not been estimated directly from these studies but a barrier height of ~0.7 eV has been estimated for the reorientation from one trigonal distortion to the other as inferred from EPR linewidth studies.[77,78] From this, a lower bound estimate of the Jahn–Teller energy can be made using the theory developed by Opik and Pryce.[81] They have calculated all of the stationary points for the lower energy surface of a T_2 state coupled to E and T_2 modes assuming only that it is sufficient to include terms up through quadratic in the displacement. As pointed out by O'Brien,[82] the stationary point they designate as "intermediate" (a combined Q_θ and Q_z mode) is actually the saddle point through which the system must go for reorientation. Their results give therefore[84] $E_{JT} \geq 4E_{\text{barrier}}$. The experimental reorientation of 0.7 eV therefore implies a Jahn–Teller energy > 2.8 eV, confirming that the Jahn–Teller energy is indeed very large. Alternatively, we can estimate the barrier height directly from our cluster calculations for comparison to the experimental value. We estimate the saddle-point energy by first minimizing the total energy vs a Q_z^α distortion alone[85] and then by further minimizing with respect to a Q_θ distortion. The energy is determined to be −3.8 eV with respect to the undistorted position, giving an estimated barrier height of 5.0 − 3.8 = 1.2 eV. In view of the simple nature of the EHT approximation, this agreement must again be considered satisfactory.

B. Donor-State Wave Function

1. Comparison to Magnetic Hyperfine Interactions

A great deal is known experimentally about the donor wave function from EPR and ENDOR studies. We have already mentioned in Sec. IV A that the trigonal Jahn–Teller distortion is clearly indicated by anisotropy in the spectrum which reveals a ⟨111⟩ axis of symmetry. In addition, strong magnetic hyperfine interactions have been observed for the nitrogen atom[75,79] (N^{14}) and for a single carbon atom[75] (via C^{13}) both of which display axial symmetry around the ⟨111⟩ defect axis. Partially resolved C^{13} satellites have also been detected and tentatively assigned to weak interactions with three other sets of carbon neighbors.[78] The quadrupole interaction for nitrogen has also been measured.[79]

The magentic hyperfine data can be used directly to infer experimental values for the donor molecular-orbital coefficients c_{vi}, Eq. (1).[86] For convenience, we rewrite Eq. (1) for the localized donor state in terms of the $2s$ and $2p$ character of each atom site,

$$\phi_D = \sum_j \left(\alpha_j^D (\psi_{2s})_j + \sum_{k=1}^{3} \beta_{jk}^D (\psi_{2pk})_j \right) . \tag{13}$$

Here k denotes the three coordinate axes and j labels each atom site. Analysis of the hyperfine data for the two principal atomic sites gives the results in Table IV, where

$$(\beta_j^D)^2 = \sum_{k=1}^{3} (\beta_{jk}^D)^2 \tag{14}$$

gives the total $2p$ character on site j. [In this analysis, values for $|\psi_{2s}(0)|^2$ and $\langle r^{-3} \rangle_{2p}$ have been estimated from published Hartree–Fock wave functions for the neutral atoms.[87] For carbon they are 2.79 and 1.69 a.u.[88] and for nitrogen they are 4.80 and 3.10 a.u.,[89] respectively.]

TABLE IV. Wave-function coefficients determined by the EHT cluster calculation for the nitrogen and nearby carbon atoms and comparison to experiment.

Site(j)	Cluster size	EHT 35 atoms	EHT 47 atoms	EHT 71 atoms	Expt. hf analysis
$N(0,0,0)$	$(\alpha_j^D)^2$	0.004	0.004	0.004	0.060
	$(\beta_j^D)^2$	0.174	0.363	0.224	0.23
$C(1,1,1)$	$(\alpha_j^D)^2$	0.029	0.022	0.017	0.066
	$(\beta_j^D)^2$	0.834	0.765	0.738	0.73
$C(\bar{1},\bar{1},1)$	$(\alpha_j^D)^2$	<0.001	<0.001	<0.001	
	$(\beta_j^D)^2$	0.003	0.010	0.003	
$C(2,2,0)$	$(\alpha_j^D)^2$	0.006	0.000	0.000	
	$(\beta_j^D)^2$	0.146	0.002	0.012	

In Table IV we also tabulate the wave-function coefficients as determined from the EHT calculation at the equilibrium 26.2% local Jahn–Teller distortion configuration. In addition to the nitrogen and the (1, 1, 1) carbon, we include the values for one each of the other nearest neighbors to the nitrogen, $(\bar{1}, \bar{1}, 1)$, and to the (1, 1, 1) carbon, (2, 2, 0). Also given are the corresponding values for large clusters where one or two extra shells of carbon atoms have been added (47- and 71-atom clusters, respectively). For these, the Jahn–Teller configuration was kept the same as for the 35-carbon-atom cluster and the extra atoms simply placed at their normal lattice positions.

Comparing these values to those determined from experiment, we note that the s character tends to be underestimated somewhat. The p character, on the other hand, which accounts for most of the wave function, is remarkably accurate. For the 71-atom cluster, the agreement is extremely good. This, of course, must be somewhat fortuitous. The experimental estimates themselves have uncertainties in them. They rely, in particular, on estimates of $|\psi_{2s}(0)|^2$ and $\langle r^{-3} \rangle_{2p}$ calculated for neutral isolated atoms and the appropriate value for the atoms in the solid may be somewhat different. Also, alternate methods for estimating these quantities for the free atoms can differ by 20–30%.[90,91] The important point to be learned from Table IV is that the wave function estimated from the present calculations is remarkably good. It is highly localized on the nitrogen and the (1, 1, 1) carbon neighbor with the major portion on the carbon.

The variation with the size of the cluster is informative and gives us some idea of the limitations imposed by the cluster size. The value on the (1, 1, 1) carbon is relatively insensitive to the size but the central nitrogen value appears to oscillate somewhat. Also we note that the rather large value found for the (2, 2, 0) site for the 35-atom cluster disappears as the next shell is added and it is no longer a surface atom. From this we conclude that the 35-atom cluster already does a rather good job of reproducing the essential features of the wave function. It can give erroneous results for neighbors which are surface atoms but otherwise the *general* character is clearly accounted for.

The tendency to underestimate the s character may result from a number of sources. In the first place, our molecular orbitals are not orthogonal to the $1s$ cores. Orthogonality would induce small admixtures of $1s$ into the orbitals which in turn could bring the predicted isotropic hyperfine interaction closer to that observed. In addition, there is evidence from the band-structure calculations of Sec. III B that our treatment of the s character

of the system is inherently less accurate. The energy at $\Gamma_{2'}$ is the most in error (Table I), being much too high in energy. This state is made up of pure s orbitals on the atoms. This indicates that, in our treatment, s character in the conduction band is very unfavorable energywise and a state made up from the conduction band will therefore tend to have low s character. Future calculations using EHT parameters adjusted to match the band structure may overcome this difficulty.

Figure 7 shows how the p character $(\beta_j^p)^2$ on the two principal atom sites varies as a function of the distortion for the 35-atom cluster. We see that the wave function leaves the nitrogen as the distortion increases but is relatively constant on the (1, 1, 1) carbon atom.[92] Also plotted in Fig. 7 are the experimentally estimated values of Table IV. They have been plotted at the predicted 26.2% distortion position, where the agreement is seen to be good.

2. *Comparison to Electric Quadrupole Interaction*

Also plotted in Fig. 7 is another monitor of the wave functions afforded by the nuclear electric quadrupole interaction. The quadrupole interaction constant P[93] is given by[94]

$$P = 3e^2qQ/4I(2I-1)\,, \tag{15}$$

where I is the spin of the nucleus, eQ its nuclear electric quadrupole moment, and eq the gradient of the electric field at the nucleus. Like the magnetic hyperfine interaction, the magnitude of the electric field gradient also receives its greatest contribution from unbalanced charge density in the orbitals of the atom itself. Unlike the magnetic hyperfine interaction, however, to which only the donor molecular orbital contributes, the electric field gradient arises from the total electron density and therefore will have contributions from all occupied molecular orbitals.

The electric field gradient at the nitrogen nucleus arising from the surrounding electronic charge density $\rho(\vec{r})$ is given by

$$eq = -e\int (3\cos^2\theta - 1) r^{-3} \rho(\vec{r})\, d\vec{r}\,, \tag{16}$$

where θ is the angle between $\vec{r}$ and the N-C (1, 1, 1) axis of symmetry. In terms of the molecular obbitals, this becomes

$$eq = -e\sum_i \langle \phi_i | (3\cos^2\theta - 1)/r^3 | \phi_i \rangle n_i\,, \tag{17}$$

where n_i is the occupancy of the ith molecular orbital. Retaining only the atomic orbitals on the nitrogen atom, this leads directly to

$$eq_N = -\tfrac{4}{5} e \langle r^{-3} \rangle_{2p} \sum_i (\beta^i_{Nx}\beta^i_{Ny} + \beta^i_{Ny}\beta^i_{Nz} + \beta^i_{Nz}\beta^i_{Nx}) n_i\,. \tag{18}$$

For a single p orbital ($n_1 = 1$, all others zero) pointing along the ⟨111⟩ direction ($\beta_{Nx} = \beta_{Ny} = \beta_{Nz} = 3^{-1/2}$), this would give

$$(eq_N)_p = -\tfrac{4}{5} e \langle r^{-3} \rangle_{2p}\,. \tag{19}$$

Therefore,

$$eq_N/(eq_N)_p = \sum_i (\beta^i_{Nx}\beta^i_{Ny} + \beta^i_{Ny}\beta^i_{Nz} + \beta^i_{Nz}\beta^i_{Nx}) n_i\,, \tag{20}$$

which expresses the field gradient conveniently in terms of the fraction unbalanced p character of the total electronic charge density on the atom.[95] Since all of the molecular-orbital coefficients are determined for each cluster calculation, (20) can be evaluated in straightforward fashion, and the result is plotted in Fig. 7. We see that although the donor-state wave function is decreasing on the nitrogen vs distortion (as evidence by the magnetic hyperfine interaction), the electric field gradient is increasing.[96]

The nitrogen quadrupole coupling constant has been measured from ENDOR studies to be[79] -3.971 MHz. To determine the electric field gradient from this [Eq. (15)] the nitrogen quadrupole moment eQ must be known. Unfortunately, it is not known accurately, estimates ranging from[97] $+0.007$ to[95] $+0.02$ ($e\times 10^{-24}$ cm^2). The problem here is that quadrupole interactions for nitrogen have only been observed in molecules or solids and, as a result, extracting the quadrupole moment ultimately falls back again to estimating the field gradient, essentially the same problem as we have here. No good *ab initio* calculations have

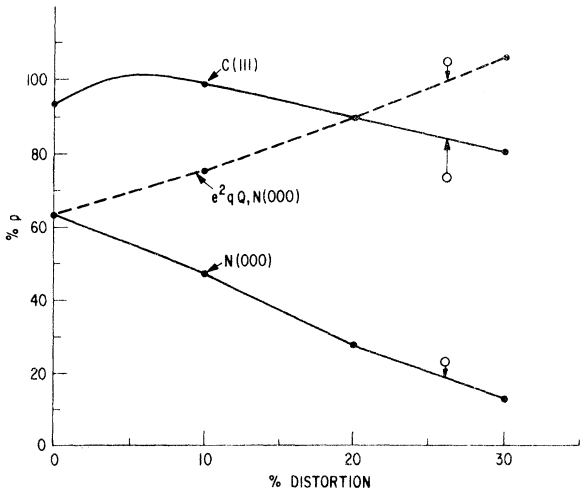

FIG. 7. Properties of the nitrogen donor wave function calculated for the 35-atom cluster and comparison with experiment. Solid lines: calculated percentage $2p$ character on the nitrogen (0, 0, 0) and its (1, 1, 1) carbon neighbor vs distortion. Dashed line: percentage unbalanced $2p$ character for the total electronic charge density on the nitrogen atom. The experimental points were derived from published EPR and ENDOR hyperfine data.

been performed to extract the quadrupole moment, the estimates in the past being relatively crude.

Therefore, we attempt to circumvent this problem as follows: We first select a molecule of known structure which has an environment for the nitrogen somewhat similar to that in diamond and for which the quadrupole interaction has been measured. For this we select hexamethylene tetramine $C_6N_4H_{12}$ which has each nitrogen bonded to three carbon atoms at approximately the tetrahedral angles, a situation similar to that of the trigonally distorted nitrogen in diamond. We then perform an EHT calculation for the molecule and calculate the field gradient via (20). We obtain

$$(C_6N_4H_{12}): \quad e^2qQ/(e^2qQ)_p = 0.903 \ . \tag{21}$$

With the measured value of $P = -3.424$ MHz for this molecule in a solid,[98] we obtain a value of

$$\tfrac{3}{4}(e^2qQ)_p = -3.793 \text{ MHz} \tag{22}$$

for the quadrupole interaction per unbalanced p electron.

Using this, the experimental value for nitrogen in diamond of $P = -3.974$ MHz gives us 1.05 fraction unbalanced p character. This point is plotted in Fig. 7, also at the 26.2% distortion position, and the agreement is seen again to be good.

The value of the quadrupole interaction per unbalanced p electron deduced from the $C_6N_4H_{12}$ calculation [Eq. (22)] can in turn be used to estimate the quadrupole moment via Eqs. (19) and (15). With the value for $\langle r^{-3}\rangle_{2p}$ used in Sec. IV B 1, the result is $Q = +0.0087\times10^{-24}$ cm^2. This is in line with other estimates[95,97,99,100] and indicates that our EHT procedure is giving reasonable results. However, we feel our procedure of using the same EHT method for calibration on a separate molecule and for the calculations of the nitrogen in diamond makes the comparison in Fig. 7 actually more meaningful than results in either of the individual systems. It is, in effect, a more accurate test than is indicated in the absolute accuracy of the quadrupole moment determination.

C. Effect of Cluster Size

We have already explored (Table IV) the effect of enlarging the cluster size on the wave function of the donor state. The effect of cluster size on the energies of the molecular orbitals is shown in Fig. 8. As in Fig. 2 for the pure carbon cluster, we show the results starting from the central nitrogen as each shell is added. The 26.2% combined trigonal distortion of the nitrogen and its four nearest carbon neighbors was held fixed throughout. It is apparent that the electrical level position for the donor state is sensitive to the size of the cluster, with the level position shifting ~1 eV in going from the 35- to the 47- and 71-atom clusters.

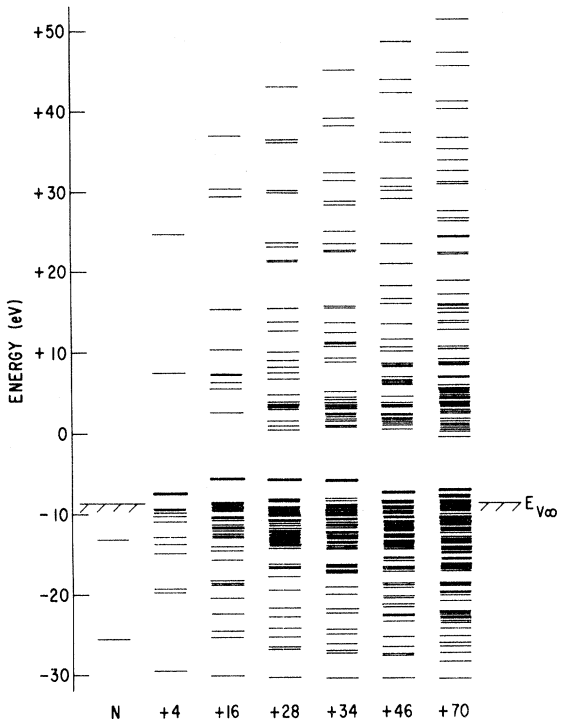

FIG. 8. Energies of the one-electron MO's for a diamond cluster containing nitrogen as a function of cluster size, starting with the central nitrogen and adding successive shells of carbon atoms up to and including the sixth-nearest-neighbor shell (+70). The 26.2% trigonal distortion of the nitrogen and its four nearest neighbors was held fixed throughout.

Figure 8 brings up a question. For the purposes of locating the electrical level position of a defect state in the gap, what should we take as the valence-band edge? In Sec. IV A we referred to the level position of the defect as measured from the "valence-band edge of the cluster," referring to the uppermost "valence-band" state for the 35-carbon-atom solution. The arguments of Sec. III A, concerning the role of surface orbitals as effectively "matching" and extending the valence-band states, gives a kind of rationale for this. Because the surface states for these small clusters tend not to be well "resolved" but rather spread through the bulk, they really are bulk states and, as such, contribute to an effective valence-band edge energy from which localized states in the bulk should be measured. In particular, we have already pointed out that the uppermost t_2 state for the 35-atom carbon cluster is spread uniformly through the cluster. On the other hand, it is clear that as the cluster size increases, the defect level will eventually approach its value for the infinite crystal and we should begin to measure its position

from the "true" valence-band edge −8.73 eV determined from the band-structure calculation.

It is obviously difficult to define a simple unambiguous procedure for handling this. At what size should the cluster be considered "small" and the "valence-band edge" of the cluster used, and at what size should it be considered large and the "true" valence-band edge be used? Table V illustrates this problem. In the table we show the level position defined in both ways vs the size of the cluster.

Table V suggests that the correct infinite cluster solution is closer to $E_V + 1.7$ eV. We interpret this to confirm that a somewhat better way to treat the 35-atom result alone is to define, as we have done in previous sections, the highest molecular orbital below the forbidden gap as the valence-band edge and measure the electrical levels from it. In doing this, the result is $E_V + 2.2$ eV, which is closer to the larger cluster result.

D. Elastic Properties and Charge Distribution

We have not discussed symmetric "breathing" modes of relaxation around the nitrogen. These may also be important. If we start with the nitrogen in the original T_d position (no trigonal distortion) and allow the four nearest carbon neighbors to relax symmetrically we find that the total EHT energy lowers dramatically as they relax outward. This is shown in the last column of Table VI. It is still decreasing at 30% expansion.

We do not trust this result for the following reason: In the table is the result of a Mulliken charge population analysis averaged over each shell of the cluster. We note that the electronic charge on the central nitrogen is increasing rapidly with distortion, having increased by $\sim 2e$ at 30% distortion. As we have discussed earlier in Sec. III D, this is a warning that EHT is giving erroneous results. Because EHT is not a self-consistent solution, there is no mechanism to prevent charge from building up on an atom. In the calculation, this lowering of energy comes from the fact that charge is being transferred to the nitrogen which has a lower ionization potential. Although this tendency is a real phenomenon and undoubtedly occurs, in the absence of a self-consistent treatment which gives a restoring force to oppose this, the results cannot be trusted. We conclude therefore that A_1 relaxation modes may be important but that the EHT treatment cannot handle them in this case. We have, therefore, not included them in our calculations.

TABLE V. Electrical level position (eV) for the nitrogen donor state vs cluster size. The valence-band edge is defined as (a) that of the cluster (E_{vc}) or (b) that of the infinite crystal ($E_{v\infty}$).

No. of atoms in cluster		5	17	29	35	47	71
(a)	$E-E_{vc}$	2.26	2.87	2.27	2.21	1.25	0.76
(b)	$E-E_{v\infty}$	1.23	3.02	2.92	2.80	1.48	1.70

No such difficulty apparently occurs for the other modes as can also be seen in Table VI. For the trigonal mode the charge on the central nitrogen is relatively constant. A Mulliken charge-population analysis serves therefore as a simple test as to whether difficulties are being encountered as a result of the differences in electronegativity of the atoms in the cluster.

Another confirmation that the elastic properties of modes (other than the A_1 mode) are realistic comes from calculating the vibrational frequency of the nitrogen at the equilibrium Jahn–Teller distortion configuration. This in turn can be compared to the experimentally observed infrared absorption spectrum that has been associated with isolated nitrogen in diamond. For the vibration parallel to the ⟨111⟩ Jahn–Teller axis, we use the Jahn–Teller mode Q_a^α, which from Table III and Eq. (10) involves mostly nitrogen motion (~75%). From the curvature of E_{tot} vs distortion at the minimum-energy point (Fig. 5), the force constant is determined to be $k = 61.5$ eV/Å^2. The vibrational frequency in turn is given by

$$\nu = (1/2\pi)\,(k/M)^{1/2}\,, \tag{23}$$

where the effective mass M for the mode is given by

$$M = (V_A^2 M_C + V_A'^2 M_N)/(V_A^2 + V_A'^2)\,. \tag{24}$$

Here M_C and M_N are the masses of the carbon and nitrogen atoms, respectively. With the values given in Table III for V_A and V_A', this gives 1110 cm^{-1} for the vibrational frequency.

Experimentally, a broad band with maximum at 1130 cm^{-1} has been identified with isolated nitrogen.[101,102] The close agreement with our value is striking and serves as additional confirmation that the proper elastic properties are being reproduced.

We have also estimated a vibrational frequency associated with motion of the nitrogen perpendicular to this axis. For this we displace the nitrogen perpendicular to the axis determining a force constant $k \sim 25$ eV/Å^2. With $M = M_N$, this indicates a perpendicular vibration frequency of 690 cm^{-1}. A broad weaker band at 850 cm^{-1} has also been observed in type Ib diamonds that can be identified with isolated nitrogen.[103,104] Our results suggest that this may be associated with modes involving the perpendicular vibration of the nitrogen.

Both of these bands are very broad because they are "resonant modes," being below the Raman frequency for diamond (1332 cm^{-1}). The modes that

TABLE VI. Charge distribution for various 35-atom-cluster calculations. The total charge resulting from a Mulliken charge-population analysis averaged over the atoms of each successive shell is shown in brackets. The unbracketed value is the departure from "uniform," as defined in the text.

System	Distortion	Typical atom site of each shell 0,0,0	1,1,1	2,2,0	3,$\bar{1}$,1	4,0,0	Total energy (eV)
35C	None	−0.1452 (4.1452)	+0.0192 (3.9808)	−0.0332 (5.0332)	+0.0618 (4.9382)	−0.0459 (6.0459)	
34C+N	None	−0.7314 (5.7314)	+0.1489 (3.8511)	−0.0266 (5.0266)	+0.0619 (4.9381)	−0.0480 (6.0480)	0
34C+N	10% trig.	−0.7396	+0.1396	−0.0239	+0.0625	−0.0469	−3.10
34C+N	20% trig.	−0.7586	+0.1263	−0.0177	+0.0622	−0.0466	−4.73
34C+N	30% trig.	−0.7759	+0.1071	−0.0101	+0.0621	−0.0462	−4.91
34C+N	+5% hydr.	−1.0232	+0.1656	−0.0076	+0.0592	−0.0465	−2.56
34C+N	+10% hydr.	−1.3537	+0.1798	+0.0193	+0.0563	−0.0454	−4.69
34C+N	+30% hydr.	−2.6313	+0.0448	+0.1679	+0.0558	−0.0386	−11.81
34C+V	None	•••	−0.4910	+0.1113	+0.0739	−0.0430	0
	+13% hydr.	•••	−0.5349	+0.1389	+0.0608	−0.0428	−1.43

we calculate are therefore broadened by coupling to allowed lattice modes. Another interesting feature of the observed infrared spectrum is a weak but very sharp band at[101–104] 1347 cm^{-1}, which is above the Raman frequency and appears to correlate with nitrogen content. This is a surprising result because the heavier nitrogen atom would not normally be expected to give rise to a true local mode with a frequency higher than the highest frequency available for the carbon atoms in the perfect lattice. We have not attempted to identify such a mode specifically in our calculations. However, we believe our general results provide a possible explanation: Because of the large Jahn–Teller distortion, the local interatomic separations are substantially altered leading to substantially modified local force constants. Some will be increased, some decreased. A local vibration, primarily carbon in character, but with increased force constants resulting from the distortion could therefore emerge as a local mode.

Finally, for completeness, let us make one further observation regarding the force constants associated with the local Jahn–Teller modes of distortion. In Sec. IV A, we determined both the Jahn–Teller coupling coefficients V_Γ and the force constants k_Γ at the undistorted T_d position. These values were given in Table III. Also shown in the table are the force constants determined for the identical modes in the 35-carbon-atom cluster, i.e., when the central atom is carbon. We note that the presence of nitrogen has altered the force constants considerably for this undistorted configuration. Our previous arguments concerning the constancy of the charge on the atoms (Table VI) would suggest that EHT is not giving us difficulty here and that the effect may be real. However, there is no way of checking it experimentally. All of our experimental checks (wave functions, energy-level positions, vibrational frequencies, etc.) refer to the equilibrium distorted configuration and there they seem to confirm that the final conclusions we are led to using EHT are essentially correct.

V. LATTICE VACANCY IN DIAMOND

Another logical defect to treat with the EHT approach is the lattice vacancy. For this, one simply removes the central atom of the cluster and solves the set of Eqs. (3). This is in many respects an ideal problem for EHT in that all atoms are identical and problems associated with partial ionicity and charge unbalance are not involved. We have previously published results of such a calculation for the 35-atom cluster.[45] In this section, we will summarize some of the more important conclusions of that work. We will also present some new results which allow an improved perspective on some aspects of the problem.

The principal result of the 35-atom cluster calculation was that a localized level of t_2 symmetry is produced in the forbidden gap when the central atom is removed. The level was found to be close to the valence-band edge with the wave function primarily localized on the four carbon atoms neighboring the vacancy. This result is shown in Fig. 9 for the levels near the valence-band edge. In Fig. 9 we also show new results for larger cluster

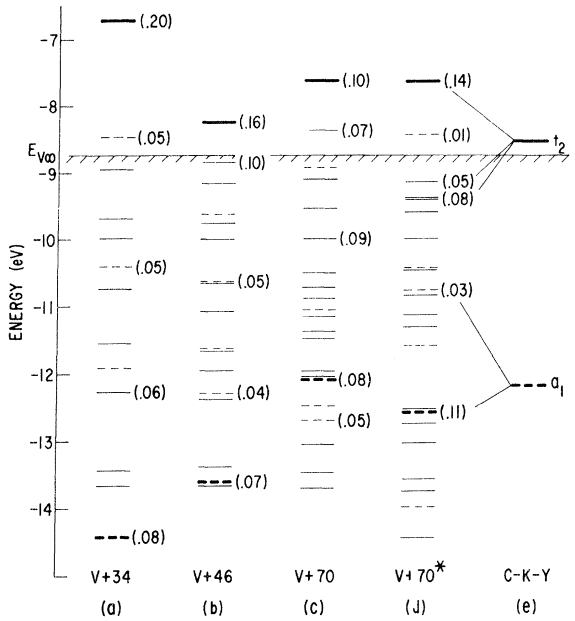

FIG. 9. a_1 (dashed lines) and t_2 (solid lines) states near the top of the valence-band edge calculated for diamond clusters containing a central atom vacancy. Shown are clusters containing (a) four, (b) five, and (c) six neighbor shells. The cluster in (d) is a 70-atom cluster constructed to have only (111) surfaces, see Ref. 58. In (e) an approximate location of the Coulson–Kearsley "defect molecule" states is indicated as inferred from (a)–(d). The numbers shown in brackets are the sum of the molecular wave-function coefficients on a (1, 1, 1) nearest-neighbor atom and serve as a measure of the localization of the state.

sizes. We see that, similar to the case of the nitrogen donor (Sec. IV), the exact position of this level is sensitive to the cluster size.

This, in turn, leads to the same degree of ambiguity in defining the level position with respect to the band edges as was found for the nitrogen donor. The level position defined with respect to both the cluster-valence-band edge and that of the infinite crystal edge is given in Table VII.

The degree of localization also changes somewhat vs cluster size as can be seen from the molecular-orbital coefficients α_j^2 and β_j^2 for the localized level in Table VII. (The value in the parentheses in Fig. 9 is $\eta_{111}^2 = \alpha_{111}^2 + \beta_{111}^2$, a measure of the total localization on each of the nearest carbon atoms.) However, the essential features clearly remain the same: In all cases, a partially filled t_2 level (occupied by two electrons for the neutral state of the vacancy) is in the gap, close to the valence-band edge and the wave function remains highly concentrated on the nearest-neighbor carbon atoms.

[In Fig. 9, for clarity, we have shown only the a_1 and t_2 levels. Since the central atom functions are of $a_1(2s)$ and $t_2(2p)$ symmetry, their removal can only alter a_1 and t_2 levels of the cluster. It is therefore sufficient to consider only these levels, for only these are related to the defect.]

Lattice relaxations of the four neighboring carbon atoms were also considered. A symmetric A_1 outward relaxation of 13%[105] was predicted. (Here the charge on the atoms remained relatively unaffected, signalling no difficulty with the A_1 breathing mode, see Sec. IV D and Table VI.) Jahn–Teller coupling coefficients to the local E and T_2 distortion modes were also estimated which indicated Jahn–Teller energies of $\sim \frac{1}{2}$ eV for the neutral state of the vacancy. However, a complex nonlinear coupling to the various modes seemed to be indicated and whether the lowest energy configuration involved a tetragonal or trigonal mode was not determined.

Another interesting feature concerning the t_2 defect wave function was that the molecular-orbital coefficients for the p functions (β_{jx}, β_{jy}, and β_{jz}) on a given near-neighbor atom (j) were not equal. In particular, for the wave function that transforms as t_{2z}, the magnitude of β_{jz} was greater than that for β_{jx} or β_{jy}. This means that if we view the localized state as made up of "dangling" orbitals from the neighboring atoms, these orbitals are not pointing into the center of the vacancy (the usual sp^3 physical chemist's concept) but rather are tilted somewhat toward the z direction. For the atom in the (1, 1, 1) position, this angle is given by

$$\theta_j = \cos^{-1}\left[\left(\sum_k \beta_{jk}\right) \Big/ \left(3\sum_k \beta_{jk}^2\right)^{1/2}\right] \quad . \tag{25}$$

TABLE VII. Properties of the T_2 localized state of the unrelaxed vacancy vs cluster size. The wave-function coefficients are given for the nearest (111) and next-nearest (2, 2, 0) neighbors to the vacancy. θ_{111} is the "tilt" of the dangling orbitals (see text), and the defect level position (eV) is given both with respect to the valence-band edge of the cluster (E_{vc}) and the infinite crystal ($E_{v\infty}$).

No. of atoms in cluster	34	46	70	70*[a]
α_{111}^2	0.010	0.006	0.005	0.005
β_{111}^2	0.189	0.154	0.098	0.130
α_{220}^2	0.001	0.000	0.000	0.000
β_{220}^2	0.048	0.006	0.013	0.011
θ_{111}	+5.4°	+18.7°	+6.7°	+10.5°
$E - E_{vc}$	1.42	0.25	0.17	0.58
$E - E_{v\infty}$	2.01	0.48	1.12	1.06

[a]Cluster with (111) surfaces, see Ref. 58.

For the 35-atom cluster this was found to be $+5.4°$. In Table VII we give the corresponding angle for the larger cluster results. The actual value varies somewhat vs cluster size but again the existence of the tilt, plus its magnitude and sign, seem to be independent of the cluster size. We take this as evidence that this is not an artifact of the finite size of the cluster or its surfaces, but rather an intrinsic feature of the defect.

In our previous publication,[45] we speculated that the origin of the tilt was the close proximity of the level to the valence-band edge. The valence-band edge at $\Gamma_{25'}$ is pure p on the atom sites and the corresponding symmetry orbital that can mix with the localized t_{2g} defect level is therefore pure p_z on the atoms. Since this orbital displays a $+54.7°$ tilt with respect to the $\langle 111 \rangle$ dangling bond directions, small admixtures into the defect wave function can serve to provide the tilt.

A test of this explanation can be obtained by shifting the defect level with respect to the band edges and monitoring the tilt. One way to accomplish this is simply to change the ionization potentials (I_μ) slightly on the four atoms surrounding the vacancy. The results of such a calculation are given in Table VIII. The correlation of the tilt with level position appears to confirm this interpretation. Much of the variation vs cluster size in Table VII probably finds explanation simply in the change of electrical level position vs size.

A. Comparison with Experiment

A direct comparison with experiment is not possible in that an unambiguous identification of the lattice vacancy in diamond does not exist.[106] On the other hand, in silicon a great deal has been learned about the lattice vacancy through EPR studies[5,107,108] and a comparison with the results in this diamond lattice material is instructive.

In silicon, the EPR results indicate that the electrical level position associated with the neutral state of the vacancy is very close to the valence-band edge. EPR in the singly ionized state (V^+) has been observed[107] and reveals a wave function which has been analyzed to have 66% ($\eta_j^2 = 0.165$) on the four nearest neighbors. A static tetragonal Jahn–Teller distortion is observed in the EPR spectrum. The Si^{29} hyperfine interactions reveal a tilt of the neighbor atom orbitals of $\theta = +7.2°$ from the $\langle 111 \rangle$ direction.

This agreement with the calculated tilt of the neighboring atom orbitals is particularly remarkable in that prior to these calculations, no satisfactory explanation for the observed tilt had been proposed. The origin was a mystery, although it had been suggested that it might result from large atomic relaxations associated with the Jahn–Teller distortion. Our calculations here demonstrate that it has nothing at all to do with the distortion but rather is a sensitive monitor of the proximity of the state to the valence-band edge. Consistent with this, V^- and other vacancy-associated centers which have been observed by EPR[6,108–115] are farther removed from the valence-band edge and display negligible tilt.

The magnitude of the Jahn–Teller effect has been estimated directly from EPR studies by analyzing the response of the silicon vacancy to externally applied uniaxial stress.[5] From these studies the Jahn–Teller stabilization energy has been estimated to be ~1.5 eV for the neutral state.[116] This is to be compared with the value $\sim \frac{1}{2}$ eV estimated from our 35-atom-cluster calculations in diamond.

TABLE VIII. Dependence of the tilt (θ_{111}) of the "dangling bonds" of the near neighbors (1,1,1) to the vacancy on the localized-defect electrical level position. The level position was altered by changing the ionization potentials I_μ on the four (1,1,1) atoms in a 34-atom-cluster calculation.

$I_\mu(111)$ (eV)		$\Delta I_\mu(111)$	$\Delta(E-E_v)$	
$2s$	$2p$	(eV)	(eV)	θ
−20.44	−11.67	−1.0	−0.31	+6.8°
−19.44	−10.67	0	0	+5.4°
−18.44	−9.67	+1.0	+0.39	+3.9°

B. Comparison to Other Theoretical Approaches

In the "defect-molecule" approach of Coulson and Kearsley,[21] and Yamaguchi[22] (CKY), a single sp^3 dangling bond pointing into the vacancy from each of the four neighboring atoms formed the basis for a molecular-orbital treatment of the vacancy in diamond. This leads immediately to four one-electron molecular orbitals, one of a_1 symmetry, and the other three forming a triply degenerate t_2 state. These molecular orbitals were then used by these authors as a basis for a many-electron configurational interaction treatment.

In our previous treatment,[45] we attempted to make a connection between the CKY "defect-molecule" approach and the large cluster results. For this purpose, we identified the t_2 and a_1 states of the 35-atom cluster which are just above the valence-band edge in Fig. 9 with the corresponding one electron "defect-molecule" states. The separation between the two states (1.8 eV for the unrelaxed vacancy, Fig. 9) was observed to be considerably less than the corresponding splitting deduced in the CKY model (~6–10 eV) and we used this as an indication of the effect of delocalization of the a_1 and t_2 states in the solid.

This has been subsequently criticized by Lark-

ins[61] who found, in extending our treatment to 41- and 46-atom clusters, that such an identification appears to break down, particularly for the a_1 state. His point is well taken, as can be seen in Fig. 9 for the larger clusters as well. There are really many t_2 and a_1 states in the cluster and more than one of each have substantial localized character. In Fig. 9 we have indicated in parentheses the localization (η_j^2) for those a_1 and t_2 states which have a large value on the nearest neighbors. All others in the cluster are significantly smaller. A simple 1:1 connection is obviously not possible.

A connection, however, is highly desirable in order to be able to relate the two approaches. Figure 9 suggests that a more meaningful way to make this connection is to define an "average" position for the localized t_2 and a_1 character of the cluster states. The progression as the cluster size increases indicates that such an average energy for the localized t_2 character would be very close to the valence-band edge at ~ -8.5 eV and the corresponding average a_1 energy would be ~ -12 eV. This is also shown in the figure. The effective splitting of these states would therefore seem to be ~3.5–4.0 eV, a value somewhat closer to the CKY result.

With this connection, it is instructive to visualize the defect as being constructed in the following simple way: First remove the central atom and construct the highly localized "defect molecule" of CKY, keeping the electronic structure of the rest of the lattice unchanged. Our preceding arguments suggest that the localized t_2 state will be close to the valence-band edge at ~ -8.5 eV. The a_1 state in turn will be ~ -12 eV. We now let the electronic states of the rest of the lattice readjust. Expressed in perturbation theory language, the nearby t_2 and a_1 states of the cluster will interact and admix with the corresponding CKY states. The "defect molecule" will tend to spill out into the cluster distributing between the various nearby t_2 and a_1 cluster states. The t_2 state that has been pushed up into the forbidden gap becomes a true "localized" state in that it is detached from the valence band. It can be considered as deriving from the original CKY t_2 state as modified by its interaction with the cluster t_2 states. It retains only part of its original near-neighbor-only character, however. The remainder of the localized character reemerges in the states with which it has interacted. The extra t_2 states in Fig. 9 which also display localized character are, therefore, simply a manifestation of the delocalization of the defect orbital in the gap. For the a_1 state, there is no true "localized" state in the usual sense of the word, the states with significant localization being "resonant" states within the band.

In summary, our cluster calculations can be interpreted to define an approximate location with respect to the perfect-lattice states for the simple one-electron a_1 and t_2 "defect molecule" states of CKY, as shown in Fig. 9. The crystal-field splitting between the two states is ~3.5–4.0 eV, which is somewhat smaller but comparable to that estimated by CKY (~5–10 eV). Delocalization of these states occurs due to interaction with the perfect-lattice states. (Approximately one-half of the localized CKY state remains for the t_2 defect state in the gap.) Since electron-electron interactions originate from terms that reflect the square of electron density, such delocalization should significantly reduce configurational interaction effects. As indicated in our previous paper, this suggests that these terms may have been significantly overestimated in the CKY treatment.

C. Migration Energy

A rough estimate of the migration energy for the vacancy can be obtained by monitoring the total EHT energy of the cluster as was done by Moore and Carlson for the graphite lattice.[39] For this we have calculated the total energy for the 34-atom cluster (a) with the vacancy in the center (0, 0, 0) position, (b) with the vacancy in the (1, 1, 1) position, and (c) with a carbon atom placed in the $(\frac{1}{2}, \frac{1}{2}, \frac{1}{2})$ position, halfway between vacancies at both the (0, 0, 0) and (1, 1, 1) sites. This last configuration was used to simulate the saddle point of the migration. Relaxations of the neighboring atoms were not treated.

The results are shown in Table IX. Our normal recipe for filling all of the cluster valence and surface states (172 electrons) gives the result in column (a). If the cluster were infinite, the value for the (1, 1, 1) or (0, 0, 0) site would be identical. We see instead that the (1, 1, 1) vacancy site is lower in energy by 1 eV, an indication that surfaces are giving us some trouble. We note that filling the levels to make the cluster neutral (136 electrons),

TABLE IX. Relative total EHT energies (eV) determined in a 34-atom-cluster calculation for configurations involved in vacancy migration.

Vacancy position	(a) 172 electrons	(b) 136 electrons
(0, 0, 0)	0	0
(1, 1, 1)	−1.0	+1.9
Saddle configuration	+2.4	+4.1
Average migration barrier	2.9	3.2

column (b), reverses the order and the difference is twice as great. This at least serves to confirm our arguments of Sec. III C that the elastic artifacts of the surfaces are reduced by our procedure.[117] However, they are still clearly evident and larger clusters with better termination of the surfaces would be required before accurate results could be expected.

It is interesting to note, however, that if we define an average barrier height between the (0, 0, 0) and (1, 1, 1) positions it is approximately 3.0 eV in either case. We, therefore, take this value as an indication of the magnitude that a more detailed calculation would give.

No direct experimental information is available for this quantity in diamond. Other theoretical estimates have given 1.85[16] and 2.02 eV.[118] The EHT cluster result is, therefore, not out of line with these other estimates. However, our experience in silicon where the experimental value of the migration activation energy[107] (0.33 eV) is much smaller than the corresponding estimates by these same approaches (1.09[16] and 1.06 eV[118]) suggests a word of caution here. It remains to be seen whether the EHT cluster approach (properly expanded to avoid surface effects and to include lattice relaxations) can be sufficiently accurate to give meaningful results for this difficult problem.

IV. SUMMARY AND CONCLUSIONS

In this paper we have described a possible theoretical approach to the problem of the deep level in a semiconductor using molecular-orbital techniques on a large cluster of host atoms surrounding the defect. As examples we have treated the nitrogen donor and the lattice vacancy in diamond in some detail. In these examples we have used the simplest representation of molecular-orbital theory, namely, extended Huckel theory.

We interpret these results to indicate that this approach is highly promising. It appears to supply all of the essential ingredients for a proper theoretical treatment, as outlined in Sec. I.

(a) If the cluster is large enough, the electrical level position of a localized defect state can be estimated with respect to the band edges. Our results demonstrate that a cluster of 35 atoms is already large enough to begin to give a meaningful connection to the states of the infinite crystal.

(b) Wave functions for the localized defect states are produced in a form which allows direct comparison with experimental information, e.g., EPR and ENDOR results. The examples we have given demonstrate that the wave functions so produced can be highly realistic.

(c) Elastic forces are implicitly included allowing local relaxation around the defect to be explored as an integral part of the treatment. The large Jahn–Teller distortion predicted for nitrogen, and confirmed by experiment, serves as a dramatic example of the necessity of including these relaxations in any treatment of the deep level problem. The complete character of the defect is changed as a result—the wave function, the electrical level position.

(d) It is a practical computational scheme. Clusters of 35 atoms can be solved in a few minutes on a modern high-speed computer.

The examples given were ones in which comparison with experiment could be made. This is an important role of theory—to make contact with and explain experimental results. Another important role of theory is to be able to supply insight and guidance in areas where no experimental information exists. One example of such an area is the complete lack of direct experimental information on the properties of the host interstitial atom in any crystal of the diamond structure (C, Si, Ge). Recently, the MO cluster approach has also been applied to this problem in diamond with the interesting conclusion that highly mobile "interstitialcy" configurations may be the most stable.[46] A charge-dependent "athermal" migration mechanism[119] along the lines recently proposed by Bourgoin[120] was suggested by the calculations. This may serve to explain much of the mystery as to why isolated interstitials have not been detected in radiation damage experiments. This work, which includes calculations on some interstitial impurities as well,[121] will be treated in detail in a subsequent publication.[122] Substitutional boron[44] and other substitutional impurities[61] have also been treated. Because of the ease with which the calculation can be performed, a wide variety of defect problems in the elemental semiconductors can now be explored by this method.

Let us now briefly review some of the limitations of the approach, how they might be avoided, and possible future extensions of the method. For this it is convenient to separate two aspects of the approach. One is the model itself—the finite cluster, problems of surfaces, etc. The other is the particular molecular-orbital technique used.

First consider the model. It is clear that larger clusters would be desirable. Unfortunately, however, the computing time increases rapidly as the number of atoms is increased. A considerable gain in this regard can be achieved by taking advantage of symmetry, i.e., factoring the secular equation first according to the irreducible representations of the symmetry group, and then solving each representation separately. We have not chosen to do this in this paper, preferring to retain the flexibility for handling arbitrary distortions. However, for very large clusters this would become mandatory. For instance, Shimizu and

Minami[123] have recently treated a cluster of 275 atoms by considering only the A_1 states in an LCAO treatment for S^+ in silicon.

However, no matter how large a cluster one takes, surfaces will still exist and are a nuisance. We believe therefore that the best solution is to remove them completely by providing periodic boundary conditions for the cluster. We are currently making such calculations on a 64-atom unit cell. The advantages are considerable. In the absence of a defect, the states of the cluster now have a direct one-to-one connection with the infinite-band states (they are, in fact, the infinite-crystal states). Upon introducing a defect, the local (and resonant) states of the defect can now be conveniently related to the perfect-lattice states from which they are "constructed," as viewed from the conventional solid-state approach such as Koster and Slater,[7] Bennemann,[16] etc. Adding periodic boundary conditions therefore serves to complete the bridge between the two extreme approaches—the "local" and "infinite-crystal" starting points—described in Sec. I. This extension thus serves to remove most of the difficulties of the finite cluster and should be used for future calculations where possible.

We now consider the molecular-orbital technique. In this paper we have considered only extended Huckel theory, which is a simple non-self-consistent semiempirical theory. Our results indicate that it does a rather good job in the elemental semiconductor diamond, where self-consistency is not important. As mentioned in the text, adjustment of the parameters to match selected symmetry points of the band structure prior to the defect calculations represents a promising extension of the method, and we are currently employing this approach for problem ' in diamond and silicon.

For partially ionic crystals, however, such as the III-V and II-VI compounds, EHT should probably not be used,[124] and a self-consistent treatment would be required. This is also true for studying charged states of defects in the elemental semiconductors. There are several molecular-orbital techniques which may be useful here. A promising new one is the self-consistent-field–scattered-wave method of Johnson[125] which employs Slater's $X\alpha$ scheme.[126] It is currently being applied to the 17-atom-cluster problem (a transition element in ZnS) considered by Birman[36] and Walter and Birman[37] and is yielding encouraging results.[127]

Finally, either with EHT or more elaborate molecular-orbital techniques, the cluster approach that we have described is still a one-electron theory and as such gives no direct information about the importance of electronic correlations. The importance of such effects in localized defects is one of current controversy,[128] although experiment has been interpreted[5,6,108] to indicate that they are not important. Our calculated wave functions could be used as a starting point for a configurational interaction treatment to estimate the importance of electronic correlation.

---

[1]C. Kittel and A. H. Mitchell, Phys. Rev. 96, 1488 (1954).

[2]W. Kohn and J. M. Luttinger, Phys. Rev. 97, 1721 (1955); 98, 915 (1955).

[3]W. Kohn, in *Solid State Physics*, edited by F. Seitz and D. Turnbull (Academic, New York, 1957), Vol. 5, p. 258.

[4]For a recent review concerned with radiation produced defects in semiconductors, see *Radiation Effects in Semiconductors*, edited by J. W. Corbett and G. D. Watkins (Gordon and Breach, London, 1971).

[5]G. D. Watkins, in *Radiation Effects in Semiconductors*, edited by F. L. Vook (Plenum, New York, 1968), p. 67.

[6]E. L. Elkin and G. D. Watkins, Phys. Rev. 174, 881 (1968).

[7]G. F. Koster and J. C. Slater, Phys. Rev. 95, 1167 (1954); 96, 1208 (1954).

[8]J. Callaway and A. J. Hughes, Phys. Rev. 156, 860 (1967).

[9]J. Callaway and A. J. Hughes, Phys. Rev. 164, 1043 (1967).

[10]J. Callaway, Phys. Rev. B 3, 2556 (1971).

[11]J. Callaway, J. Math. Phys. 5, 783 (1964).

[12]N. J. Parada, Phys. Rev. B 3, 2042 (1971).

[13]F. Bassani, G. Iadonisi, and B. Preziosi, Phys. Rev. 186, 735 (1969).

[14]M. Lannoo and P. Lenglart, J. Chem. Phys. Solids 30, 2409 (1969).

[15]M. D. Rouhani, M. Lannoo, and P. Lenglart, J. Phys. (Paris) 31, 597 (1970).

[16]K. H. Bennemann, Phys. Rev. 137, A1497 (1965); *Conference on Calculation of the Properties of Vacancies and Interstitials, Skyland, Va.*, 1966, NBS Misc. Publ. No. 287 (U.S. GPO, Washington, D. C., 1967), p. 127.

[17]J. L. Beeby, Proc. Roy. Soc. (London) A302, 113 (1967).

[18]K. H. Johnson, Intern. J. Quantum Chem. 25, 233 (1968).

[19]K. H. Johnson and F. C. Smith, Jr., in *Computational Methods in Band Theory*, edited by P. M. Marcus, J. F. Janak, and A. R. Williams (Plenum, New York, 1971), p. 377.

[20]P. Goossens and P. Phariseau, Physica 45, 575 (1970); 45, 587 (1970).

[21]C. A. Coulson and M. J. Kearsley, Proc. Roy. Soc. (London) A241, 433 (1957).

[22]T. Yamaguchi, J. Phys. Soc. Japan 17, 1359 (1962).

[23]T. Yamaguchi, J. Phys. Soc. Japan 18, 368 (1963).

[24]C. A. Coulson and F. P. Larkins, J. Phys. Chem. Solids 30, 1963 (1969).

[25]C. A. Coulson and F. P. Larkins, J. Phys. Chem. Solids 32, 2245 (1971).

[26]F. P. Larkins, J. Phys. Chem. Solids 32, 965 (1971).

[27]J. Friedel, M. Lannoo, and G. Leman, Phys. Rev.

164, 1056 (1967).
[28]A. B. Lidiard and A. M. Stoneham, in *Science and Technology of Industrial Diamonds* (Industrial Diamond Information Bureau, London, 1967), Vol. I, p. 1.
[29]M. Lannoo and A. M. Stoneham, J. Phys. Chem. Solids 29, 1987 (1968).
[30]F. P. Larkins and A. M. Stoneham, J. Phys. C 4, 143 (1971); 4, 154 (1971).
[31]F. P. Larkins, J. Phys. Chem. Solids 32, 2123 (1971).
[32]B. S. Gourary and A. E. Fein, J. Appl. Phys. 33, 331 (1962).
[33]A. M. Stoneham, Proc. Phys. Soc. (London) 88, 135 (1966).
[34]R. P. Messmer and G. D. Watkins, Phys. Rev. Letters 25, 656 (1970).
[35]T. Inui and Y. Uemura, Prog. Theoret. Phys. (Kyoto) 5, 252 (1950).
[36]J. L. Birman, in *Proceedings of the International Conference on Luminescence*, edited by G. Szigeti (Akademai Kiado, Budapest, 1968), p. 919.
[37]W. Walter and J. L. Birman, in *II-VI Semiconducting Compounds*, edited by D. G. Thomas (Benjamin, New York, 1967), p. 89.
[38]M. Wolfsberg and L. Helmholtz, J. Chem. Phys. 20, 837 (1952).
[39]E. B. Moore, Jr. and C. M. Carlson, Solid State Commun. 4, 47 (1965).
[40]R. Hoffmann, J. Chem. Phys. 39, 1397 (1963).
[41]See also R. S. Mulliken, J. Chim. Phys. 46, 497 (1959); J. Chim. Phys. 46, 675 (1959); and Ref. 38.
[42]C. C. J. Roothaan, Rev. Mod. Phys. 23, 69 (1951).
[43]R. C. Chaney, C. C. Lin, and E. E. Lafon, Phys. Rev. B 3, 459 (1971).
[44]G. D. Watkins and R. P. Messmer, in *Proceedings of the Tenth International Conference on the Physics of Semiconductors, Cambridge, Mass.*, 1970, edited by S. P. Keller, J. C. Hensel, and F. Stern (U.S. AEC, Oak Ridge, Tenn., 1970), p. 623.
[45]R. P. Messmer and G. D. Watkins, in *Radiation Effects in Semiconductors*, edited by J. W. Corbett and G. D. Watkins (Gordon and Breach, London, 1971), p. 23.
[46]G. D. Watkins, R. P. Messmer, C. Weigel, D. Peak, and J. W. Corbett, Phys. Rev. Letters 27, 1573 (1971).
[47]Discussions of the approximations which are necessary to obtain the EHT equations from Hartree–Fock theory as well as consideration of the extent of validity of these approximations are given in Ref. 55 and in F. P. Boer, M. D. Newton, and W. N. Lipscomb, Proc. Natl. Acad. Sci. U. S. 52, 890 (1964); M. D. Newton, F. P. Boer, and W. N. Lipscomb, J. Am. Chem. Soc. 88, 2353 (1966), as well as some references contained therein. An alternative formulation has been given by T. L. Gilbert, in *Sigma Molecular Orbital Theory*, edited by O. Sinanoğlu and K. Wiberg (Yale U.P., New Haven, Conn., 1970), p. 249.
[48]The valence orbital ionization potentials I_μ are obtained from experimental atomic ionization potentials as described in Ref. 49.
[49]J. A. Pople and G. A. Segal, J. Chem. Phys. 43, S136 (1965).
[50]J. C. Slater, Phys. Rev. 36, 57 (1930).
[51]L. C. Allen and J. D. Russell, J. Chem. Phys. 46, 1029 (1967).
[52]L. C. Allen, in *Sigma Molecular Orbital Theory*, edited by O. Sinanoğlu and K. B. Wiberg (Yale U.P., New Haven, Conn., 1970), p. 227.
[53]J. C. Slater, *Quantum Theory of Molecules and Solids* (McGraw-Hill, New York, 1963), Vol. I, pp. 107-109.
[54]J. Goodisman, J. Am. Chem. Soc. 91, 6552 (1969).
[55]G. Blyholder and C. A. Coulson, Theoret. Chim. Acta 10, 316 (1968).
[56]The program used in these calculations was a modified version of programs generally available from the Quantum Chemistry Program Exchange, Department of Chemistry, Indiana University, Bloomington, Ind., and originally written by Hoffmann (QCPE 30) and Carlson and Moore (QCPE 64). The modifications that have been introduced increase the efficiency of the program, reducing the required core storage and computing time.
[57]R. P. Messmer, Chem. Phys. Letters 11, 589 (1971).
[58]Formed from the "spherical" 71-atom cluster by removing 12 of the 24 sixth neighbors $(4,2,\bar{2})$ and inserting the 12 (5,1,1) seventh neighbors.
[59]This is also true for the 71*-atom cluster, which, like the 35-atom cluster, has only {111} surfaces. Such clusters are attractive ones in that they have the minimum number of surface "dangling bonds" for a given number of atoms. In addition, these bonds are pointing parallel to each other on each surface (Fig. 1), providing minimum mutual overlap. It is probably for this reason that these clusters reveal less evidence for "surface states" and tend to display fewer states above the valence-band edge.
[60]E. B. Moore, Jr. and C. M. Carlson, Phys. Rev. B 4, 2063 (1971).
[61]F. P. Larkins, J. Phys. C 4, 3065 (1971); 4, 3077 (1971).
[62]G. S. Painter, D. E. Ellis, and A. R. Lubinsky, Phys. Rev. B 4, 3610 (1971).
[63]L. A. Hemstreet, Jr., C. Y. Fong, and M. L. Cohen, Phys. Rev. B 2, 2054 (1970).
[64]C. Kittel, *Introduction to Solid State Physics*, 3rd ed. (Wiley, New York, 1966), Chap. 4.
[65]By allowing the two sublattices to relax with respect to each other in the trigonal distortion, we obtain an estimate for the internal displacement factor ξ (Refs. 66 and 67) of 0.13. No experimental determination exists for this parameter in diamond but a value of 0.21 has been inferred from the elastic constants using a valence-force-field model (Ref. 68).
[66]A. Segmuller and H. R. Neyer, Physik Kondensierten Materie 4, 63 (1965).
[67]L. Kleinman, Phys. Rev. 128, 2614 (1962).
[68]R. M. Martin, Phys. Rev. B 1, 4005 (1970).
[69]L. Pauling, *The Nature of the Chemical Bond*, 2nd ed. (Cornell U.P., Ithaca, 1945), p. 64.
[70]R. T. Sanderson, *Chemical Periodicity* (Rheinhold, New York, 1960), p. 34.
[71]R. S. Mulliken, J. Chem. Phys. 23, 1933 (1955).
[72]P. Denham, E. C. Lightowlers, and P. J. Dean, Phys. Rev. 161, 762 (1967).
[73]P. J. Dean, Phys. Rev. 139, A588 (1965).
[74]R. G. Farrer [Solid State Commun. 7, 685 (1969)] has recently reported results which he interprets as locating the nitrogen donor level at 1.7 eV below the *conduction band*. If his samples were partially compensated, a likely possibility, then his results could equally well be interpreted as locating the level with respect to the

valence band, a result consistent with the general consensus (Refs. 72 and 73).

[75]W. V. Smith, P. P. Sorokin, I. L. Gelles, and G. J. Lasher, Phys. Rev. 115, 1546 (1959).

[76]J. H. N. Loubser and L. Du Preez, Brit. J. Appl. Phys. 16, 457 (1965).

[77]L. A. Shul'man, I. M. Zaritskii, and G. A. Podzyarei, Fiz. Tverd. Tela 8, 2307 (1966) [Soviet Phys.-Solid State 8, 1842 (1967)].

[78]J. H. Loubser and W. P. van Ryneveld, Brit. J. Appl. Phys. 18, 1029 (1967).

[79]R. J. Cook and D. H. Whiffen, Proc. Roy. Soc. (London) A295, 99 (1966).

[80]M. D. Sturge, in *Solid State Physics*, edited by F. Seitz, D. Turnbull, and H. Ehrenreich (Academic, New York, 1967), Vol. 20, p. 91.

[81]U. Opik and M. H. L. Pryce, Proc. Roy. Soc. (London) A238, 425 (1957).

[82]Mary C. M. O'Brien, Phys. Rev. 187, 407 (1969).

[83]Strictly speaking Eq. (11) should also contain terms in $Q_a^\alpha Q_a^\beta$, $(Q_a^\beta)^2$, etc., because the Q_a^α and Q_a^β are not *normal* modes. This means in turn that the lowest-energy configuration will have some Q_a^β admixed into it via these coupling terms. For our purposes, however, Eq. (11) should be adequate to probe out the essential features of the problem.

[84]If there is zero coupling to tetragonal modes, $E_{JT} = 4E_{\text{barrier}}$. A finite coupling to the tetragonal modes makes $E_{JT} > 4E_{\text{barrier}}$.

[85]Here again we use the combinations of the two Q_z and Q_z' modes as given by Eq. (10).

[86]See, for example, G. D. Watkins and J. W. Corbett, Phys. Rev. 121, 1001 (1961).

[87]E. Clementi, IBM J. Res. Develop. Suppl. 9, 2 (1965).

[88]G. Malli and S. Fraga, Theoret. Chim. Acta (Berlin) 6, 54 (1966).

[89]S. Fraga and G. Malli, University of Alberta Division of Theoretical Chemistry, Technical Report No. TC-6601 (unpublished).

[90]C. M. Hurd and P. Coodin, J. Phys. Chem. Solids 28, 523 (1966).

[91]R. G. Barnes and W. V. Smith, Phys. Rev. 93, 95 (1954).

[92]The percentage on the (1, 1, 1) carbon is not defined at 0% distortion, because it depends upon the particular linear combination of the degenerate t_2 orbitals selected. As soon as an infinitesimal distortion occurs, however, this sets the wave function and gives the value shown.

[93]As defined in the spin-Hamiltonian term $P[I_z^2 - I(I+1)/3]$.

[94]T. P. Das and E. L. Hahn, *Nuclear Quadrupole Resonance Spectroscopy* (Academic, New York, 1958), p. 5.

[95]C. H. Townes and B. P. Dailey, J. Chem. Phys. 17, 782 (1949).

[96]The field gradient is also not defined at 0% distortion; see Ref. 92. The value plotted is that for an infinitesimal trigonal distortion that sets the wave function.

[97]A. Bassompierre, Discussions Faraday Soc. 19, 260 (1955).

[98]G. D. Watkins and R. V. Pound, Phys. Rev. 85, 1062 (1952). The value we take represents the extrapolated estimate for 0 °K.

[99]J. Sheridan and W. Gordy, Phys. Rev. 79, 513 (1950).

[100]C. C. Lin, Phys. Rev. 119, 1027 (1960).

[101]H. B. Dyer, F. A. Raal, L. Du Preez, and J. H. N. Loubser, Phil. Mag. 11, 763 (1965).

[102]R. M. Chrenko, H. M. Strong, and R. E. Tuft, Phil. Mag. 23, 313 (1971).

[103]J. F. Angress, A. R. Goodwin, and S. D. Smith, Proc. Roy. Soc. (London) A308, 111 (1968).

[104]R. M. Chrenko (unpublished).

[105]This is the amplitude of the normalized A_1 breathing mode measured in terms of the nearest-neighbor distance. Each atom therefore moves outward by 6.5% of the nearest-neighbor distance (1.54 Å).

[106]J. A. Baldwin [Phys. Rev. Letters 10, 220 (1963)] reports a center in irradiated diamond which he attributes to the isolated vacancy in diamond. Our results are also consistent with the inferred properties of that center.

[107]G. D. Watkins, J. Phys. Soc. Japan 18, Suppl. II 22 (1963).

[108]G. D. Watkins, in *Radiation Damage in Semiconductors* (Dunod, Paris, 1965), p. 97.

[109]G. D. Watkins and J. W. Corbett, Phys. Rev. 121, 1001 (1961).

[110]G. D. Watkins and J. W. Corbett, Phys. Rev. 134, A1359 (1964).

[111]G. D. Watkins and J. W. Corbett, Phys. Rev. 138, A543 (1965).

[112]G. D. Watkins, Phys. Rev. 155, 802 (1967).

[113]M. Nisenoff and H. Y. Fan, Phys. Rev. 128, 1605 (1962).

[114]W. Jung and G. S. Newell, Phys. Rev. 132, 648 (1963).

[115]K. L. Brower, in *Radiation Effects in Semiconductors*, edited by J. W. Corbett and G. D. Watkins (Gordon and Breach, London, 1971), p. 189.

[116]G. D. Watkins (unpublished).

[117]G. D. Watkins and R. P. Messmer, Phys. Rev. B 4, 2066 (1971).

[118]R. A. Swalin, J. Phys. Chem. Solids 18, 290 (1961).

[119]J. S. Koehler and R. E. McKeighen, Bull. Am. Phys. Soc. II, 16, 396 (1971).

[120]J. C. Bourgoin and J. W. Corbett, Phys. Letters 38A, 135 (1972).

[121]C. Weigel, D. Peak, J. W. Corbett, G. D. Watkins, and R. P. Messmer, Bull. Am. Phys. Soc. II 16, 501 (1971).

[122]C. Weigel, D. Peak, J. W. Corbett, G. D. Watkins, and R. P. Messmer (unpublished).

[123]T. Shimizu and K. Minami, Phys. Status Solidi (b) 48, K181 (1971).

[124]Part of the difficulty experienced by Birman *et al.* (Refs. 36 and 37) (negative values for some of the K's required to fit experiment) could stem from this.

[125]K. H. Johnson and F. C. Smith, Jr., Phys. Rev. B 5, 831 (1972).

[126]J. C. Slater and K. H. Johnson, Phys. Rev. B 5, 844 (1972).

[127]K. H. Johnson, in *Advances in Quantum Chemistry*, edited by P. O. Lowdin (Academic, New York, 1973), Vol. 7.

[128]See, for instance, A. M. Stoneham, in *Radiation Effects in Semiconductors*, edited by J. W. Corbett and G. D. Watkins (Gordon and Breach, London, 1971), p. 7.